Part III: Pre-Earthquake Seismic Phenomena

8

Short-Term Foreshocks and Earthquake Prediction

Gerassimos Papadopoulos, George Minadakis, and Katerina Orfanogiannaki

ABSTRACT

Foreshock recognition before main shocks depends on various factors, e.g. geophysical, catalog completeness, foreshock definition, and spatiotemporal windows. Foreshocks move towards the main shock epicenter as the event approaches, their number increases as time to the event decreases, and their *b*-value decreases. However, only in a very few single foreshock sequences have these three-dimensional patterns been recognized at the same time, e.g. before the 2009 L' Aquila (Italy) earthquake (*Mw* 6.3) and the 2010, 2014 and 2015 major earthquakes (*Mw* 8+) in the Chilean subduction zone. For the first time we found statistically significant three-dimensional foreshock patterns before two small-to-moderate earthquakes occurring on 4 March 2012 (*Mw* 5.2) and 3 July 2013 (*Mw* 4.8) in Athos and Polyphyto, northern Greece. The marked similarity of the patterns found before strong and major earthquakes indicates that the foreshock process is scale invariant in a wide magnitude range. It is likely that the process is independent of the faulting type, at least for dip-slip faulting. There is also a trend of the main shock magnitude to scale with the foreshock area. These findings imply that foreshock activity is likely governed by a universal pattern, which may also reflect universality in the deformation process thus opening new directions for utilization of the foreshock pattern in earthquake prediction.

8.1. INTRODUCTION

Short-term foreshocks increase the probability for the occurrence of a future strong main shock [*Yamashina*, 1981; *Jones*, 1985b; *Agnew and Jones*, 1991; *Console et al.*, 1993; *Savage and DePolo*, 1993; *Dodge et al.*, 1995; *Michael*, 2012]. Therefore, foreshock activity has been considered as one of the most promising precursory phenomena for the prediction of the main shock [e.g. *Wyss*, 1997; *Vidale et al.*, 2001]. For example, the short-term prediction of the large (*M* 7.2) earthquake of 4 February 1975 in Haicheng, China, was based on several precursory phenomena, particularly short-term foreshocks [*Raleigh et al.*, 1977; *Scholz*, 1977; *Jones et al.*, 1982]. Short-term foreshocks are considered in a time frame varying from minutes up to several months before the main shock.

Superiority of foreshock activity as compared to other candidate earthquake precursors is apparent because (a) foreshocks occur exactly in the area that is highly stressed before the main shock and (b) the foreshock three-dimensional distribution in the space, time, and size domains likely follows a certain pattern.

In spite of the progress noted so far as regards the precursory value of foreshocks, there still remain some very important issues of uncertainty. The first regards foreshock occurrence pattern: why are some main shocks preceded by foreshocks while others are not? Of relevance to this question of foreshock incidence concerns whether they are associated with large main shocks only, or also with moderate or even small main shocks. The second

Institute of Geodynamics, National Observatory of Athens, Athens, Greece

Pre-Earthquake Processes: A Multidisciplinary Approach to Earthquake Prediction Studies, Geophysical Monograph 234, First Edition. Edited by Dimitar Ouzounov, Sergey Pulinets, Katsumi Hattori, and Patrick Taylor.

important issue refers to the three-dimensional pattern that governs foreshock activity: do all foreshock sequences have a similar pattern? Is this pattern dependent on the main shock size and faulting type? Importantly, is it possible to use three-dimensional foreshock pattern to discriminate foreshocks from other types of spatiotemporal seismicity clusters, like swarms and aftershocks? Is such a pattern useful for the prediction of the main shock? In this chapter we examine these fundamental issues using seismicity data from several earthquake areas worldwide.

8.2. FORESHOCK RATE

One of the very early reports on the rate of foreshocks preceding main shocks was that of *Imamura* [1937, p. 78], who reported that the number of earthquakes that are ushered in by foreshocks barely reaches 20% of the total number. He added, however, that with the sensitive seismometers now in use this proportion would increase. In the aftermath of the prediction of the 4 February 1975, Haicheng (China) earthquake, increased interest was shown in the predictive value of foreshocks. As a consequence, studies focused on whether foreshocks are a common occurrence. In a global review of large ($M \geq 7$) shallow earthquakes, *Jones and Molnar* [1976] found that 44% in the National Oceanic and Atmospheric Administration list had at least one foreshock. Yet, they proposed that this percentage was too low an estimate since foreshock recognition is strongly influenced by seismograph coverage and event cataloging. In another global review, *Seggern* [1981] found a foreshock rate of < 20% for main shocks of magnitude ≥ 5.8, but again this was dependent on earthquake monitoring capabilities and foreshock definition.

In addition, contradictory results were also found in several seismic regions of the Earth. In California and in the western cordillera of USA, estimations of the foreshock rate varied from 35% [*Jones*, 1985a], to 50% [*Agnew and Jones*, 1991], and to 60% [*Doser*, 1989], depending on the time period and the main shock magnitude threshold considered as well as on the spatiotemporal foreshock definition adopted. In the North Pacific region large interplate earthquakes are preceded by foreshock sequences at a rate of 70% [*Bouchon et al.*, 2013]. On the Chinese mainland, *Chen et al.* [1999] found that only 5% of the 159 main shocks ($M > 1.5$) had foreshocks in the period 1966–1996. However, this result was strongly influenced by the *a priori* foreshock definition adopted by the authors of that paper; foreshock occurrence was considered within 5 days and 20 km of the main shock, with occurrence rate exceeding ten events per day with $M \geq 1.5$. At the other extreme, for the thrust fault system of Chengkung, eastern Taiwan, all six of the larger earthquakes ($M_L \geq 5$) occurring between 1992 and 2003 had foreshocks at a distance of only a few kilometers within just a few days of the main shock [*Lin*, 2004].

Foreshock rate dependence on predefined spatiotemporal windows is also indicated by several studies in various parts of the world, such as in Japan [*Yamashina*, 1981; *Maeda*, 1999; *Imoto*, 2005], *Kamchatka* [*Sobolev*, 2000], New Zealand [*Merrifield et al.*, 2004], Albania [*Peçi et al.*, 1999], Italy and Greece [*Di Luccio et al.*, 1997; *Console et al.*, 1993, *Papadopoulos et al.*, 2000]. A characteristic example on how foreshock recognition depends on the foreshock definition adopted is provided by the case of the 12 November 1999 Düzce earthquake (*Mw* 7.1) of the North Anatolian Fault. *Wu et al.* [2014] investigated for foreshocks preceding that large earthquake within only ~ 65 h before and within 20 km of the main shock. No foreshock activity was found. To use foreshocks as a potential tool for short-term prediction of the main shock it is of great importance to discriminate between foreshocks and other types of seismicity clusters, e.g. swarms and main-shock–aftershock sequences [e.g. *Ogata et al.*, 1996], but this again depends on the foreshock definition.

The foreshock rate depends also on the completeness of the earthquake catalog [e.g. *Yamaoka et al.*, 1999]; small seismic events, including foreshocks, usually are not included in standard catalogs produced by routine daily seismic analysis; an example is provided by the strong ($Mw = 5.8$) earthquake of 20 October 2005 in the eastern Aegean Sea, Greece, which was reported by *Papadopoulos et al.* [2006]. No foreshocks were recognized in the standard catalog produced by the National Observatory of Athens, Greece, however, analysis of the records at one local station installed close to the epicenter showed that at least 50 foreshocks of small magnitude preceded the main shock.

Incidence or not of foreshocks very likely depends on a variety of geophysical factors, such as the style of faulting, focal depth, and degree of small-scale crustal heterogeneity [e.g. *Abercrombie and Mori*, 1996; *Cheng and Wong*, 2016]. This may explain at least in part why only some main shocks are preceded by short-term foreshocks. On the other hand, catalog incompleteness as well as the adoption of very narrow spatiotemporal limits when searching for foreshocks may lead to foreshock events being missed. Therefore, these important issues should be taken into account in the investigation of foreshock patterns in the space–time–size domains.

8.3. FORESHOCK PATTERNS

The possibility that foreshock sequences perhaps follow recognizable patterns in the space, time, and size domains was explored as early as the 1960s. *Suyehiro et al.* [1964] observed an increase in seismicity before the

great Chilean earthquake (*Mw* 9.5) of 22 May 1960, as well as a decrease in *b*-value [*Suyehiro*, 1966]. Increase in precursory signals of crustal failure is also supported by the pioneering laboratory experiments on material fracture conducted by *Mogi* [1963a,b] and *Scholz* [1968]. Subsequently, it was verified that the foreshock increase in time as the earthquake approached follows a pattern of acceleration [e.g. *Papazachos*, 1975; *Ishida and Kanamori*, 1978*; Kagan and Knopoff*, 1978; *Jones and Molnar*, 1979; *Maeda*, 1999; *Yamaoka et al*., 1999; *Papadopoulos et al*., 2000, 2010]. Averaging of data over several foreshock sequences revealed that the foreshock acceleration process fits well with a power-law distribution [e.g. *Jones and Molnar*, 1979]; an observation further supported by numerical modeling using spring-blocks [e.g. *Hainzl et al*., 1999] as well as by modeling of analytical damage mechanics [e.g. *Main*, 2000; *Yamashita and Knopoff*, 2007]. In addition, it has been found that foreshocks tend to move towards the main shock epicenter [e.g. *Engdahl and Kisslinger*, 1978; *Chen et al*., 1999; *Papadopoulos et al*., 2010; *Lippiello et al*., 2012].

In the size domain the critical parameter is *b*, which is the slope of the straight line in the magnitude–frequency (or G–R; Gutenberg–Richter) relation [*Ishimoto and Iida*, 1939; *Gutenberg and Richter*, 1944]

$$\log N = a - bM \tag{8.1}$$

where N is the cumulative number of events of magnitude equal to or larger than M and a and b are variables determined by the data. Therefore, b is an experimentally observed macroscopic variable measuring the ratio of small-magnitude events relative to large-magnitude events. At the global scale of seismicity, the *b*-value was found to be around unity [e.g. *Frohlich and Davis*, 1993; *Schorlemmer et al*., 2005]. However, locally or even regionally this parameter varies due to its strong dependence on stress-loading conditions [*Mogi*, 1963a; *Scholz*, 1968] and on crustal heterogeneity [e.g. *Abercrombie and Mori*, 1996]. A low value of b indicates enhancement in higher magnitude events, high stress conditions, and/or increased material heterogeneity. Inversely, a high *b*-value is interpreted as evidence for enhancement of events of smaller magnitudes, low stress, and/or decreased material heterogeneity. Therefore, b could be considered as a stress meter that depends inversely on differential stress [e.g. *Schorlemmer et al*., 2005]. From simulations on Olami–Feder–Christensen spring-block models, *Avlonitis and Papadopoulos* [2014] showed that the low values of b experimentally observed in foreshock sequences can be modeled by a process of material softening in the seismogenic volume. If foreshock activity is a signature of high stress conditions, then it may be expected that the b value would decrease with respect to background seismicity and aftershocks. This is exactly the finding of several authors, including *Mogi* [1963a,b, 1985], *Suyehiro and Sekiya* [1972], *Papazachos* [1975], *Jones and Molnar* [1979], *Main et al*. [1989], *Molchan et al*. [1999], *Chan et al*. [2012], *Kato et al*. [2012], and *Nanjo et al*. [2012].

Until the occurrence of the strong (*Mw* 6.3) L' Aquila, central Italy, earthquake of 6 April 2009, no single earthquake sequence was known to be characterized by the presence of foreshock patterns in the three domains at the same time. In single foreshock sequences, patterns in only one or two domains were found, thus making questionable their universality. In addition, only in a few cases were the precursory seismicity changes, determined as foreshock activities, tested for their statistical significance. These issues are of crucial importance for organizing a research strategy aiming to investigate three-dimensional foreshock patterns. In this endeavor two alternative approaches may be followed. The first is to examine global or regional earthquake catalogs looking for foreshocks before a set of strong earthquakes, potentially considered as main shocks, with the adoption of a magnitude value cut-off and of pre-selected spatiotemporal limits. Global and regional catalogs are very inhomogeneous, however, particularly in the magnitude domain and are characterized by much variation in their completeness in space and time domains. In addition, as described earlier, foreshock rate depends directly on the definition of foreshock, while preselection of narrow spatiotemporal limits may lead to artificial elimination of foreshocks. Such difficulties may explain the contradictory results obtained about the level of foreshock rate in various seismogenic regions of the Earth.

Another alternative is to investigate good examples of single foreshock sequences in sufficiently complete catalogs of earthquakes using a low cut-off value for magnitude. Such catalogs can be found in areas of dense, continuous monitoring coverage, and are compiled on the basis of standard seismic analysis procedures. This strategy was applied to the L'Aquila 2009 earthquake, which is the first single foreshock sequence where three-dimensional foreshock patterns were recognized to occur at the same time, and which have been tested for statistical significance using the national seismic catalog of Italy's National Institute of Geophysics and Volcanology (INGV) [*Papadopoulos et al*., 2010; *Daskalaki et al*., 2016] (Table 8.1).

Another excellent example is the great Iquique, Chile, earthquake (*Mw* 8.1) of 1 April 2014. Several studies supported that foreshock activity very likely controlled the initiation of the great earthquake through gradual unlocking of the plate boundary [*Brodsky and Lay*, 2014; *Kato and Nakagawa*, 2014; *Lay et al*., 2014; *Ruiz et al*., 2014; *Schurr et al*., 2014; *Yagi et al*., 2014; *Bedford et al*., 2015; *Meng et al*., 2015; *Duputel et al*., 2015]. Different opinions, however, were expressed regarding the initiation time of the activity and the extent

Table 8.1 Parameters of earthquake sequences, E, having significant foreshock patterns in the domains of space, time and magnitude before the earthquake events examined in the present paper.

Event	Date	Time	*Mw*	h (km)	Latitude	Longitude	M_c	M_f	Radius[d] (km)	d_w	d_s
L' Aquila, Italy[a]	6 April 2009	01:32:39	6.3	10	42.42°N	13.39°E	1.3	4.0	15	150	10
Maule, Chile[b]	27 February 2010	06:34:08	8.8	30	36.29°S	73.24°W	3.0	5.6	170	103	-
Athos, Greece[c]	4 March 2012	03:31:07	5.2	23	40.13°N	24.05°E	1.4	5.1	10	53	18
Polyphyto, Greece[c]	3 July 2013	13:28:23	4.8	20	40.14°N	21.87°E	1.1	4.7	10	236	1.1
Iquique, Chile[b]	1 April 2014	23:46:45	8.1	39	19.57°S	70.91°W	2.6	6.7	65	53	17
Illapel, Chile[b]	16 September 2015	22:54:31	8.4	23	31.64°S	71.74°W	3.0	5.3	50	108	-

Mw, moment magnitude; *h*, focal depth; M_c, cut-off magnitude; M_f, maximum foreshock magnitude; d_w, duration in days of weak foreshock stage; d_s, duration in days of strong foreshock stage.
[a]*Papadopoulos et al*. [2010].
[b]*Papadopoulos and Minadakis* [2016].
[c]Present study).
[d]Radius of circular foreshock area considered for the strong foreshock stage; if only weak foreshock stage was detected this was taken into account.

of the foreshock area. For example, *Schurr et al*. [2014] proposed that foreshock activity was developed at least 500 days or so before the main shock, but *Ruiz et al*. [2014] found that the precursory foreshock activity started on 4 January 2014. As for the foreshock area, *Schurr et al*. [2014] suggested that it extended from 19.00°S to 21.00°S (ca. 220 km) along the subduction zone strike, while *Ruiz et al*. [2014] determined a foreshock area that spans ~150 km along the strike of the subduction zone. Such discrepancies can be explained by the realization that interest was focused on investigating how foreshocks contributed to the stress accumulation before the great Iquique 2014 main shock rather than on three-dimensional foreshock patterns and their deviation from randomness through testing for statistical significance; only the activity rate variation was statistically tested by *Schurr et al*. [2014], who found significant changes during the 250 days leading up to the main shock.

Systematic investigation of three-dimensional patterns revealed that the great Iquique 2014 earthquake was preceded by statistically significant patterns quite similar to those found before the L'Aquila 2009 main shock [*Papadopoulos and Minadakis*, 2016] (Table 8.1). Of particular importance is the difference in magnitude and the seismotectonic regimes associated with the two earthquakes: crustal normal faulting for L'Aquila 2009, subduction-related thrust for Iquique 2014. Similar three-dimensional foreshock patterns preceded the great Chilean earthquakes of Maule, 27 February 2010 (*Mw* 8.8) and Illapel, 16 September 2015 (*Mw* 8.4) [*Papadopoulos and Minadakis*, 2016] (Table 8.1). However, in these cases only weak foreshock activity was detected, likely because of catalog incompleteness.

Later in this chapter we examine two additional good examples, those of small-to-moderate earthquakes (*Mw* 5.2 and *Mw* 4.8) that occurred in Greece in 2012 and 2013 (Table 8.1). These cases, along with those of L'Aquila in 2009 and of Chile in 2010, 2014 and 2015, cover a wide spectrum for the main shock magnitude and represent various seismic areas of the world characterized by different seismotectonic regimes.

8.4. METHOD OF ANALYSIS AND COMPUTATIONAL NOTES

Seismicity analysis for the *a posteriori* identification of precursory foreshock patterns was performed using the in-house developed FORMA (FOReshock–Main shock–Aftershock) software that has been explained elsewhere [e.g. *Papadopoulos et al*., 2010; *Papadopoulos and Minadakis*, 2016]. Therefore, we only briefly describe the method and the computational details that we followed in our analysis.

Foreshock patterns were investigated in the space, time and size (magnitude) domains. In the space domain, the Euclidean distance, D, of earthquake epicenters from the main shock epicenter was used as a metric of the seismicity spatial variation. The seismicity (activity) rate, r, and the b-value of the G–R relation are metrics used to detect changes in the time and size domains, respectively. At the beginning of the investigation procedure we selected sufficiently wide enough spatiotemporal windows so as to avoid missing possible foreshocks. We gradually narrowed the windows until significant space–time seismicity changes, if any, were detected and the target area was determined. Once a seismicity cluster was detected as candidate foreshock activity, we put forward the hypothesis that the entire time interval selected for analysis comprised two different but sequential states of seismicity, the background period of seismicity and the foreshock (testing) period. The statistical significance of changes in D and r were tested with the z-test. Changes in b were checked with the test of *Utsu* [1966, 1992], which measures the statistical significance of the difference in the b-value between two earthquake samples. According to the Utsu test, the probability, P, that two samples may come from the same population is calculated by

$$P \approx \exp\left[-\left(\mathrm{d}A/2\right)-2\right] \tag{8.2}$$

where $\mathrm{d}A$ is a function of the number of events and of the b-values in the two samples. The lower the metric P, the higher the significance level.

Our assumption is that detection of an increase in r and decrease in D and b indicate foreshock activity. We considered that the foreshock activity is weak or strong when the three precursory seismicity changes are significant (level more than 90%) or highly significant (level more 95%), respectively. Also, the significant change of only two out of three parameters may indicate weak foreshock activity.

Particular attention is paid to the b-value estimation since this parameter is quite sensitive to the computational techniques used. We adopted the maximum likelihood approximation of *Aki* [1965] for calculation of b, hereafter denoted as b_{ML}. For reasons of comparison we also calculated b_{GR} by applying the weighted least-square method to the G–R magnitude distribution. The parameter b, however, depends on the magnitude cut-off, M_c, and therefore was calculated for various levels of M_c. Also of interest was to examine the time evolution of b in the target area and so a conditional backward windowing technique was applied. An initial value of b_{ML} was calculated starting with a window comprising the last n events just prior to the main shock. The process was repeated for the next n events sliding backwards

with steps of 1 event until the whole process reached the last n events from the beginning of the entire time interval selected for analysis. A value of $n = 100$ was selected if enough earthquake events were contained in the catalog; otherwise a lower value of n was selected appropriately. Another condition included in this procedure is that $\Delta = M_{max} - M_{min} > 1.4$, since it was found [*Papazachos*, 1974] that when $M_{max} - M_{min} < 1.4$, the calculation of b becomes quite unstable: where M_{max} and M_{min} are the maximum and minimum magnitudes inserted in the earthquake sample under examination. When the condition $\Delta > 1.4$ was not fulfilled in the backward windowing technique, the calculation was repeated by increasing the window with a step of 1 event at a time until the condition was fulfilled.

Another way of examining b-value variation is to consider the variation of mean magnitude, $<M>$, since it has been shown that in an earthquake sample $<M>$ is a function of the inverse of b [*Utsu*, 1965; *Lomnitz*, 1966; *Hamilton*, 1967]. Therefore, $<M>$ was also calculated with the backward windowing technique.

8.5. FORESHOCKS PRECEDING SMALL-TO-MODERATE GREEK EARTHQUAKES

We have applied our method of seismicity analysis to two seismic sequences recorded in Greece in 2012 and 2013. What the two sequences have in common is that they culminated with main shocks of moderate magnitudes: on 4 March 2012 with *Mw* 5.2 and on 3 July 2013 with *Mw* 4.8. The other common feature is the relatively low magnitude cut-off in the earthquake catalog, which as we explain later was found to be as low as 1.40 and 1.10, respectively, and favors seismicity analysis and testing for statistical significance.

The earthquake catalog used was taken from the Institute of Geodynamics, National Observatory of Athens, Greece (http://www.gein.noa.gr/en/ and http://bbnet.gein.noa.gr/ HL/database; last accessed 17 May 2016), which operates the national seismograph system in the country. In the National Observatory at Athens (NOA), the recorded data are sent to the National Data Center via the SeedLink protocol, where they are processed automatically (SeisComp3 analysis suite) and analyzed manually by operators in a 24/7 mode (Nanometrics processing suite). We used the catalog compiled after manual processing. Since the particular suite for manual processing was established on 1 February 2011, changes were caused in the homogeneity of the earthquake catalog as regards magnitude determination. Therefore, the date 1 February 2011 was considered as the beginning of the background seismicity period in the present analysis. Staff at NOA calculated moment magnitude, *Mw*, and local magnitude, M_L, following standard procedures, the details of which can be found in links in the above website.

8.5.1. Athos, Northern Greece, 4 March 2012, *Mw* 5.2

On 4 March 2012, a moderate earthquake of magnitude *Mw* 5.2/M_L 5.0 occurred offshore Athos Peninsula, northern Greece (Figure 8.1, Table 8.1). This earthquake was preceded by another moderate earthquake occurring on 14 February 2012, 01:34:38 UTC, and measuring *Mw* 5.1/M_L 5.0. Since the two epicenters are nearly identical, hereafter the epicenter of the strongest event is considered as the common epicenter for both events and is called the target point.

Precursory seismicity changes were investigated initially in a circular area of radius 50 km around the target point for the period extending from 1 February 2011 up to the occurrence of the 4 March 2012 event (Figure 8.1). The investigation revealed that from 22 December 2011 the seismicity clustered in a narrow area at a distance of no more than 20 km from the target point (Figure 8.1). Before the *Mw* 5.1 event of 14 February 2012 the activity clustered at a distance of about 10 km from the target point. After a temporary expansion of the activity at a distance ranging from about 10 km to 20 km, the activity moved even closer to the main event target point at distances between only 4 km and 10 km (Figures 8.2 and 8.3). This result is independent of the number of earthquake events used to calculate the Euclidean mean distance, D, of earthquake epicenters from the target point (Figure 8.3).

Based on the spatial clustering of the earthquake activity, seismicity changes were further investigated in the time and size domains in a target area of radius 20 km around the target point. The background period was taken from 1 February 2011 up to 21 December 2011, while the testing period was considered to extend from 22 December 2011 up to the occurrence of the 4 March 2012 main event. Completeness analysis of the earthquake catalog, based on the G–R diagrams, showed that the magnitude cut-off could be taken as low as $M_c = 1.40$ (Figure 8.4, left). For $M_c = 1.40$ the seismicity rate gradually increased from $r_b = 0.17$ events day^{-1} in the period of background seismicity to $r_f = 5.21$ events day^{-1} in the foreshock period (Figure 8.5). This increase was found significant at the level of 100%.

It should not pass unnoticed that there was a pause in seismicity during the first 12 days of February 2011 (Figure 8.5). We checked whether this was an artifact owing to a temporary lack of station records, but this can be rejected since the stations of the national seismograph system in North Greece were operating normally during that period, recording seismic events in a

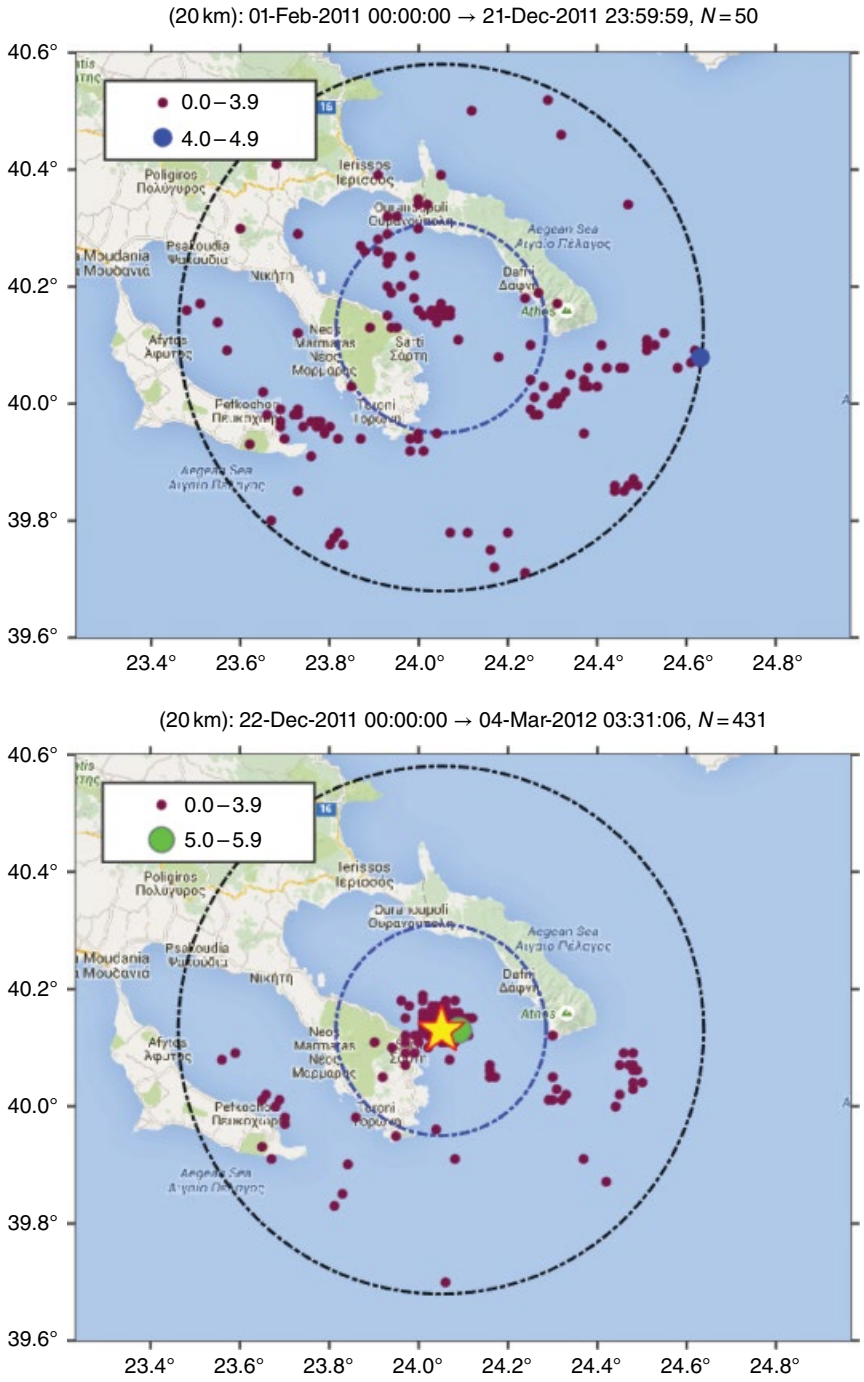

Figure 8.1 Earthquake epicenter plots in the area of Athos, northern Aegean Sea, Greece, for two time periods: (top) from 1 February 2011 to 21 December 2011 and (bottom) from 22 December 2011 to 4 March 2012. Circles are radii of 50 and 20 km from the epicenter (target point) of the 4 March 2012 main event (star). After 21 December 2011 the seismicity was significantly clustered close to the main event epicenter.

wide magnitude range and occurring outside the target area. Therefore, we concluded that the temporary pause in seismicity, which we call foreshock quiescence, was of natural origin.

The G–R diagram (Figure 8.4) clearly illustrates that the value of b_{ML}, equal to 1.22 in the background period, reduced to 0.77 in the foreshock period. This difference is highly significant, as indicated by the Utsu test (equation

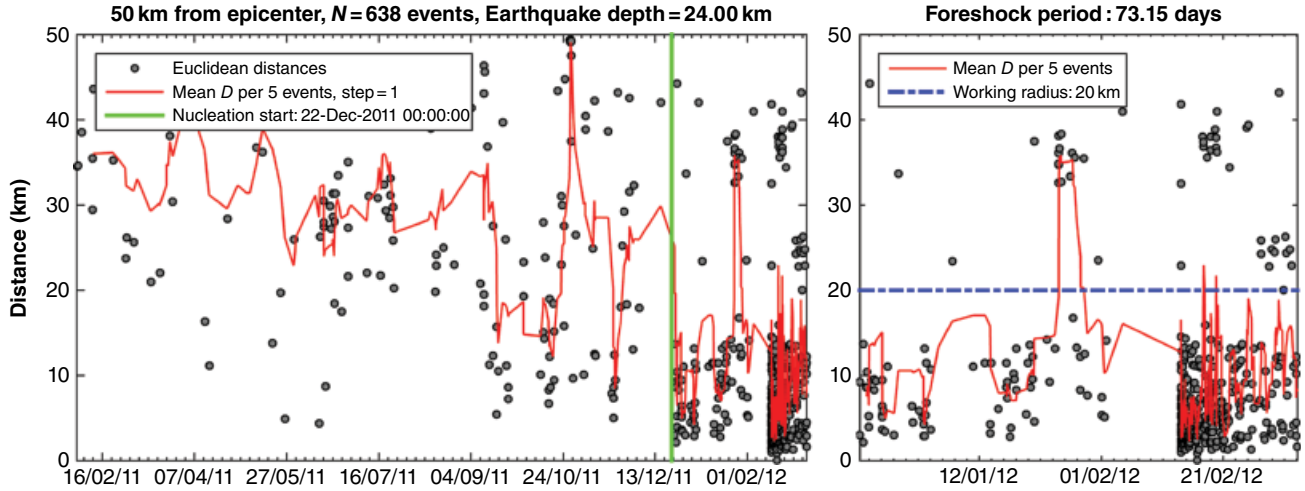

Figure 8.2 Time variation of the average Euclidean distance, *D*, of epicenters from that of the main event of 4 March 2012 (target point). At each point of time, *D* was calculated as the average of five events.

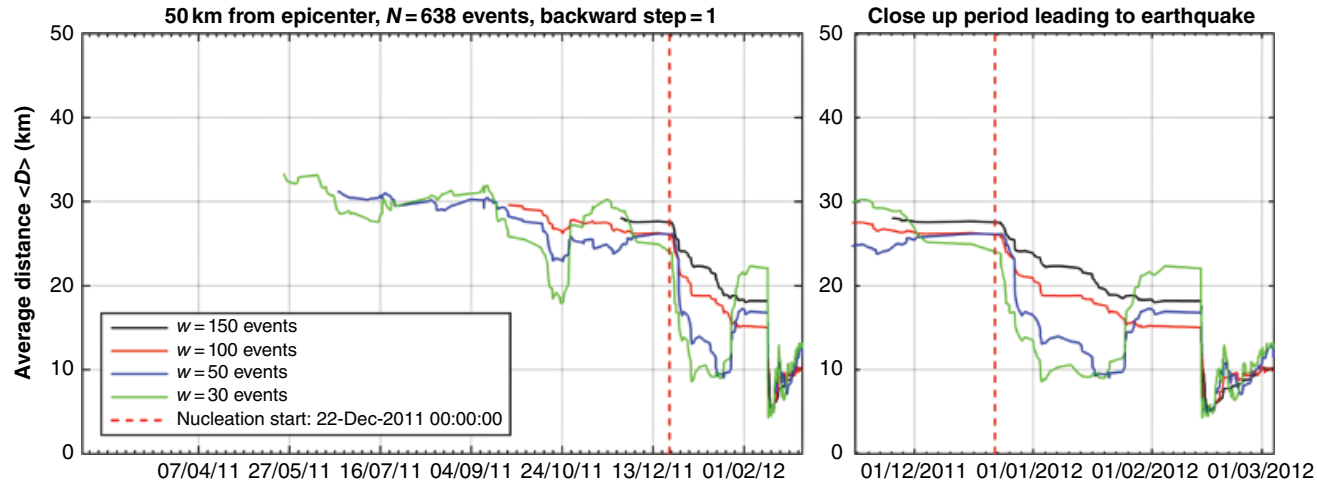

Figure 8.3 Time variation of the average Euclidean distance, *D*, of epicenters from the target point. At each point of time, *D* was calculated with the backward technique as the average of 30, 50, 100, or 150 events starting from the origin time of the 4 March 2012 main event and using a step of 1 event.

8.2) which found $P = 0.008$. It is noteworthy that the b_{ML} decrease does not depend on the magnitude cut-off considered (Figure 8.4, bottom). To further check the b_{ML} time variation, a backward testing technique was performed (Figure 8.6). For reasons of comparison the time variation of the mean magnitude, $<M>$, was also tested with the same technique. As might be expected, the two variations are consistent with each other in the sense that they follow inverse patterns. The b_{ML} decrease and the corresponding increase of $<M>$ from the beginning of the testing period up to the occurrence on 14 February 2012 of the strongest event in the testing (foreshock) period, are quite evident. However, after that event the patterns for both b_{ML} and $<M>$ temporarily reversed. At the same time the activity rate increased significantly showing an Omori-like distribution similar to the aftershock time distribution that followed the main event of 4 March 2012 (Figure 8.7). This aftershock-like feature is consistent with the notion that activity expanded spatially, as previously noted. An explanation could be that immediately after the event of 14 February 2012 the earthquake population was enhanced in smaller magnitude events and this temporarily enhancement caused the *b*-value to increase to around its level during the background seismicity. Soon after, however, both parameters again exhibited changes to be expected in foreshock sequences, i.e., b_{ML} decreased and $<M>$ increased during about the last 2 weeks before the main event occurred (Figure 8.6).

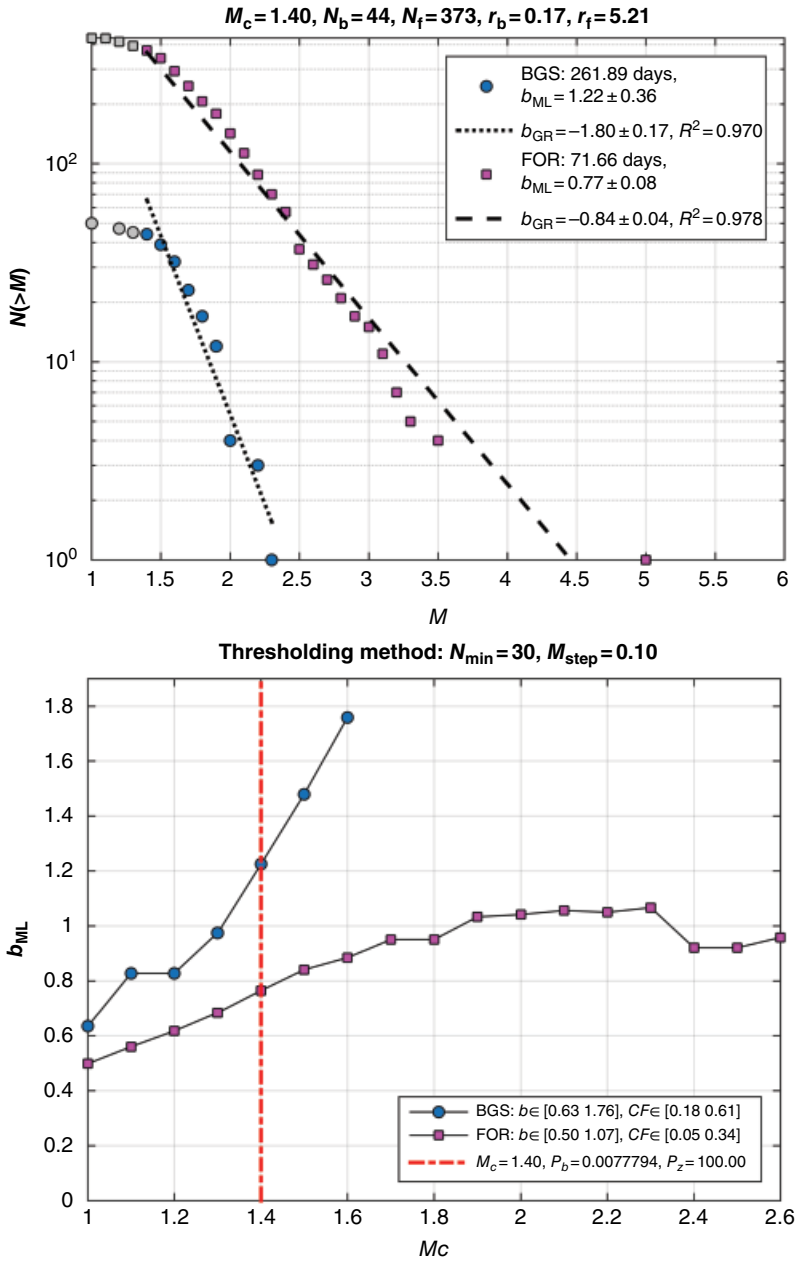

Figure 8.4 (Top) Magnitude–frequency (G–R) distribution of earthquakes occurring in the background seismicity period (BGS) and the foreshock period (FOR) before the main event of 4 March 2012: M_c, cut-off magnitude; N_b, number of events in BGS; N_f, number of events in FOR; r_b, seismicity rate in BGS; r_f, seismicity rate in foreshock period; N_{min}, minimum number of events; b_{ML} and b_{GR} are calculated by the maximum-likelihood and the weighted least-squares methods, respectively. In FOR the b_{ML} remains lower than that in BGS for different M_c levels (bottom). Calculation performed for $N_{min} = 30$ with a magnitude step of 0.10: *CF*, confidence interval; P_b, Utsu probability test; P_z, *z* probability-test.

Since the magnitude difference between the main shock and the strongest foreshock is as small as 0.1 and falls within the error limits it may be argued that the later was the main shock and the former was a strong aftershock. It therefore is of interest to check closer the seismicity features from the onset of the suggested foreshock period on 22 December 2011 up to the occurrence of the 14 February 2012 event. We found that the spatial cluster observed before the 14 February 2012 earthquake (Figure 8.7) was associated with an activity rate increase from $r_b = 0.17$ events day^{-1} in the background period to $r_f = 1.59$ events day^{-1} in the foreshock period (Figure 8.8).

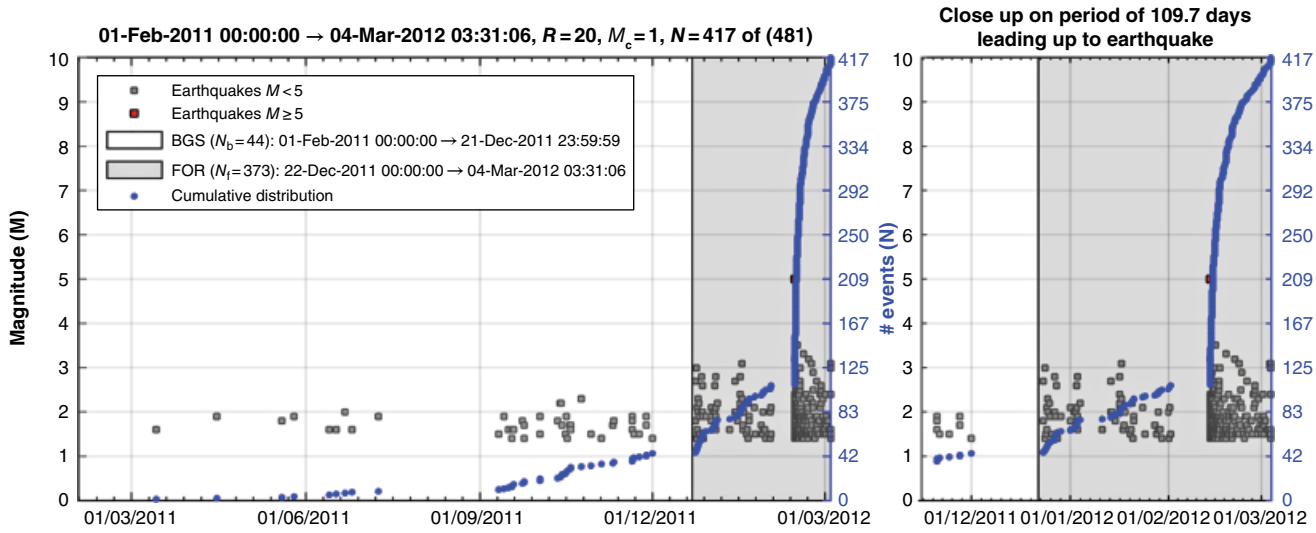

Figure 8.5 Cumulative number of earthquake events of magnitude $M \geq M_c = 1.40$ occurring in the target area ($R = 20$ km) around the epicenter of the 4 March 2012 main event (target point). See Figure 8.4 for notation.

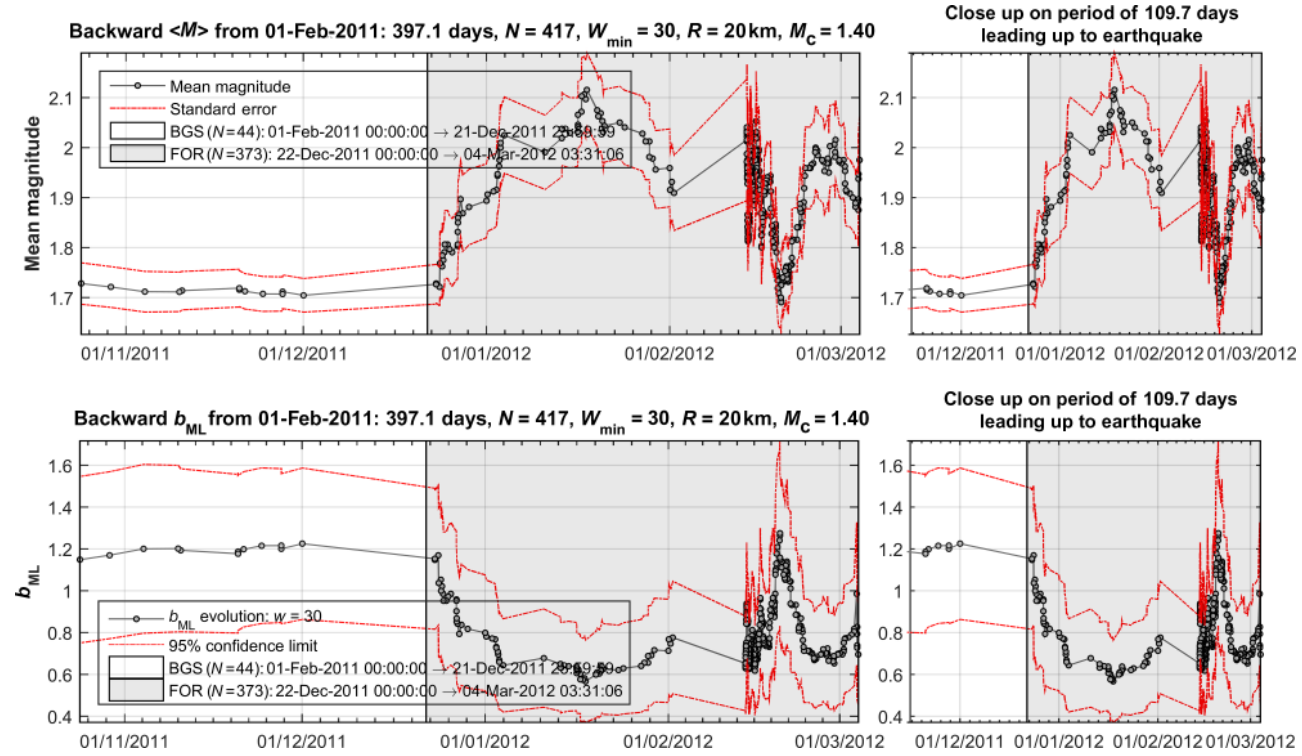

Figure 8.6 Time variation of (upper) mean magnitude, <*M*>, and (lower) b_{ML} of earthquake events of $M \geq M_c = 1.40$ occurring in the target area ($R = 20$ km) around the target point. Both parameters were calculated with the backward technique by taking window $w = 30$ events starting from the origin time of the 4 March 2012 main event and using a step of 1 event.

This change was significant at the 99.99% level. At the same time, the value of b_{ML} decreased from 1.22 to 0.70, a highly significant change at the $P = 0.008$ level (Figure 8.9, top), and this gradual decrease in b_{ML} was accompanied by a gradual increase of $< M >$ (Figure 8.10). Again the b_{ML} reduction was independent of the magnitude cut-off considered (Figure 8.9, bottom). From these findings it transpires that the 14 February 2012 event was preceded by three-dimensional foreshock patterns similar to those that preceded the 4 March 2012 earthquake. It is

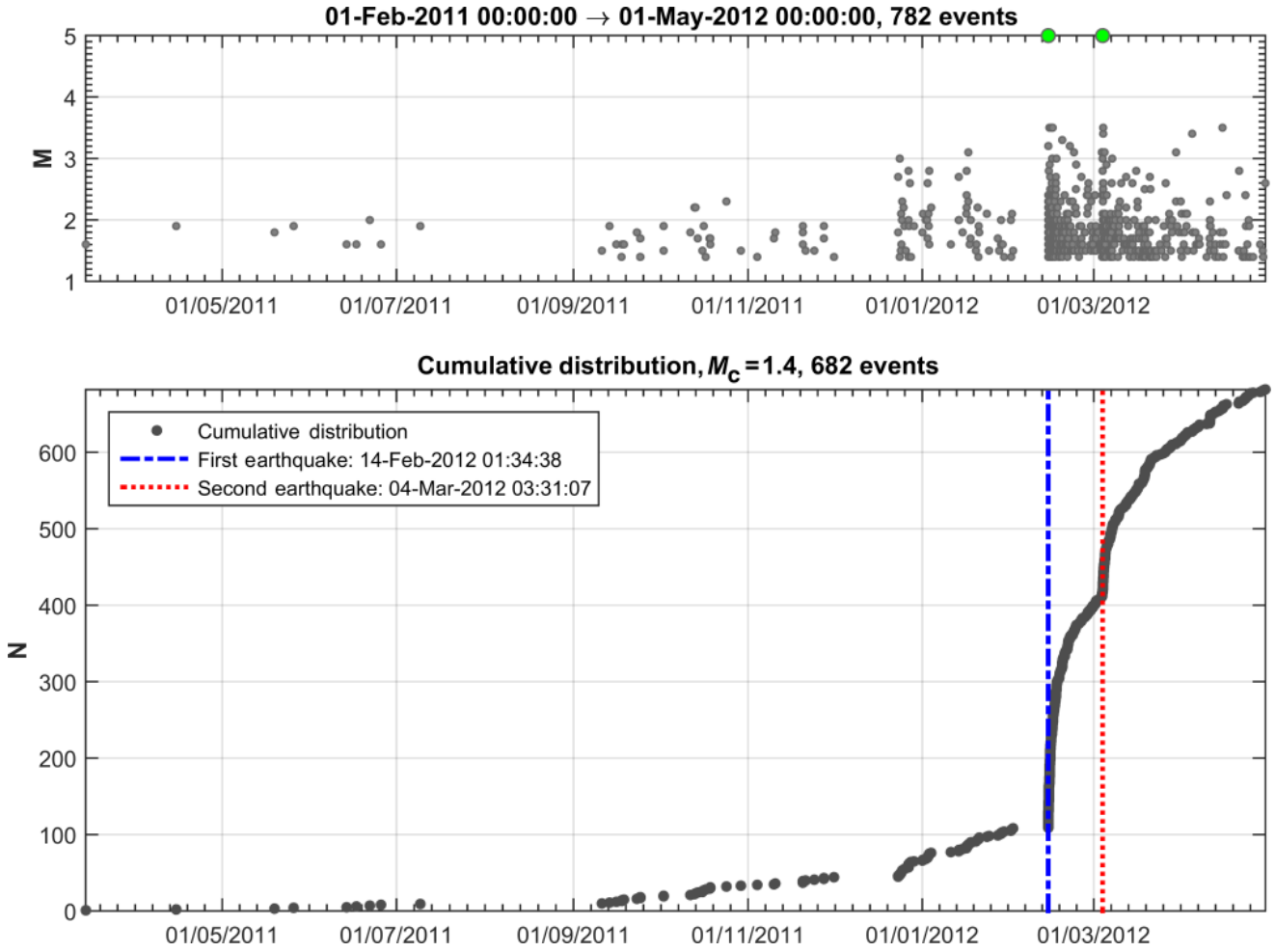

Figure 8.7 Cumulative number, N, of earthquake events of magnitude $M \geq M_c = 1.40$ occurring until the end of April 2012 in the target area ($R = 20$ km) around the target point. Vertical blue and red dotted bars show the origin times of the strong foreshock of 14 February 2012 and of the main shock, respectively. See Figure 8.4 for notation. (*See electronic version for color representation.*)

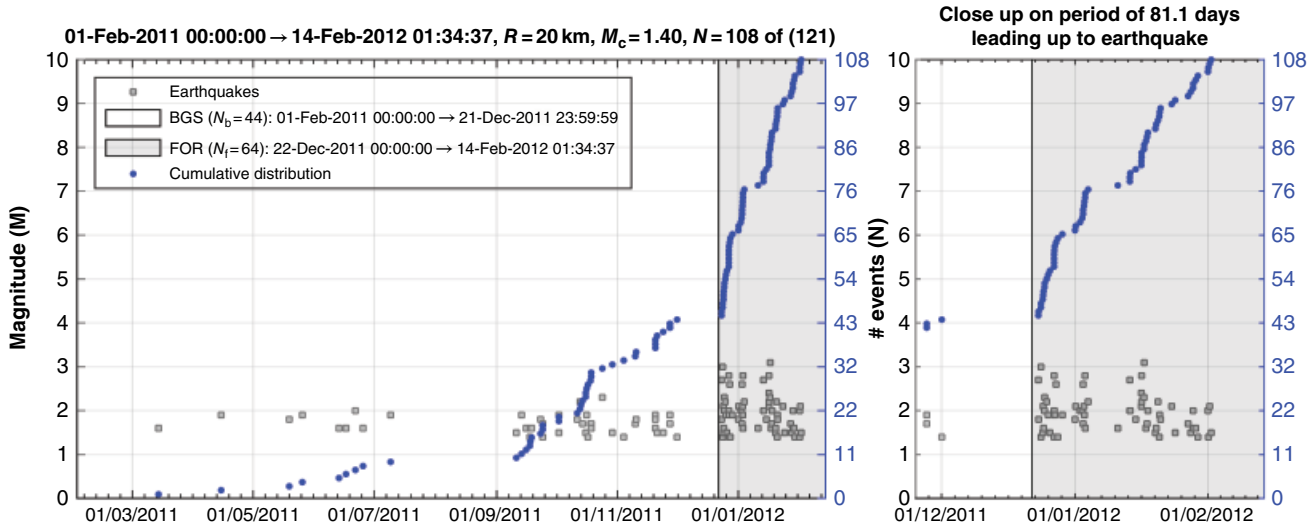

Figure 8.8 Cumulative number of earthquake events of $M \geq M_c = 1.40$ occurring in the target area ($R = 20$ km) around the target point in the BGS and FOR periods; see Figure 8.4 for notation. The 14 February 2012 earthquake coincides with the right-hand vertical axis of both panels.

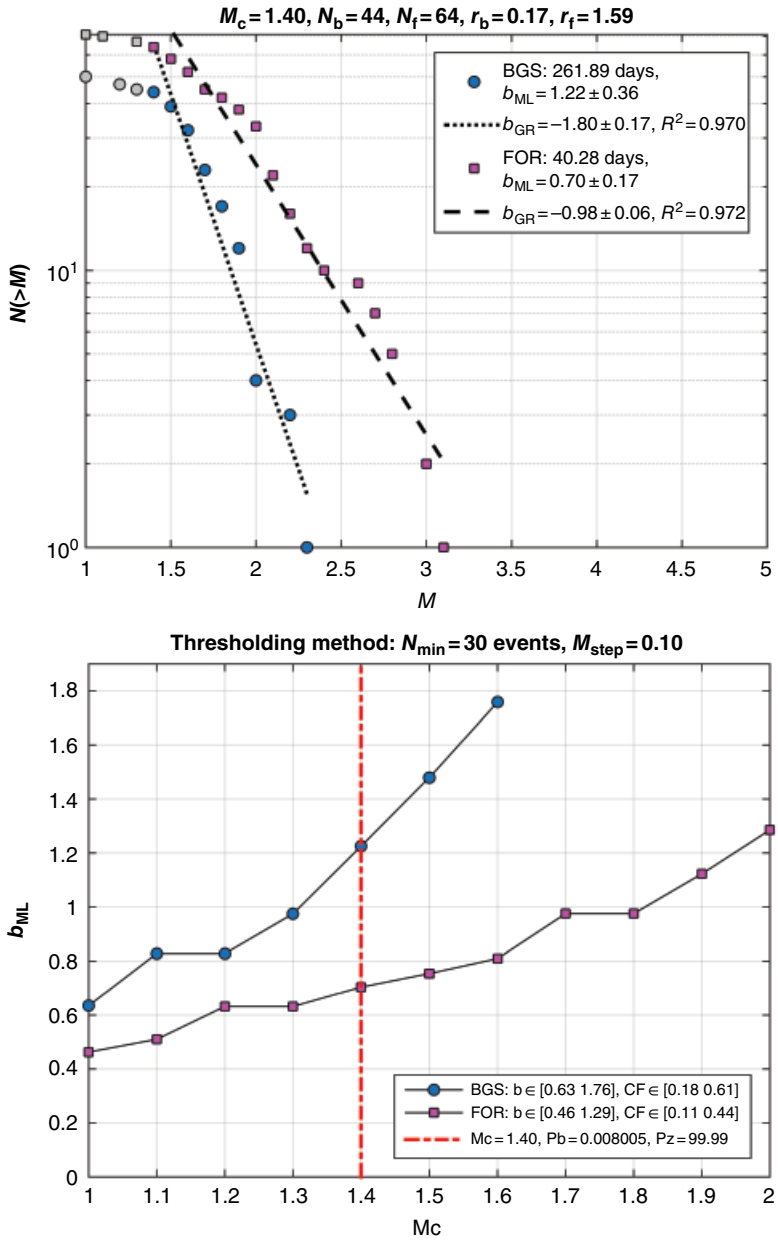

Figure 8.9 (Top) Magnitude–frequency (G–R) distribution of earthquakes occurring in the BGS and FOR periods before the *Mw* 5.1 earthquake of 14 February 2012. See Figure 8.4 for notation. In the FOR period the b_{ML} remained lower than that in the BGS period for different M_c levels (bottom). Calculation performed for $N_{min} = 30$ with a magnitude step of 0.10.

noteworthy that foreshock quiescence also happened before the 14 February 2012 event.

From the seismicity patterns detected before the 4 March 2012 earthquake we concluded that this is another good example of a main shock preceded by foreshock sequence characterized by significant three-dimensional precursory patterns. This case is important for the additional reason that although the main shock was of moderate size its foreshock patterns are quite similar to those observed before larger main shocks, such as the *Mw* 6.3 earthquake of 6 April 2009 in L'Aquila, Italy, and the *Mw* 8.1 earthquake of 1 April 2014 in Iquique, Chile. An additional similarity is the development of the foreshock sequence in two main stages: a weak foreshock stage and a strong foreshock stage. In the Athos case the stage of weak foreshock activity lasted from 22 December 2011 up to the occurrence of the 14 February 2012 (*Mw* 5.1) strong foreshock, which was also preceded by similar

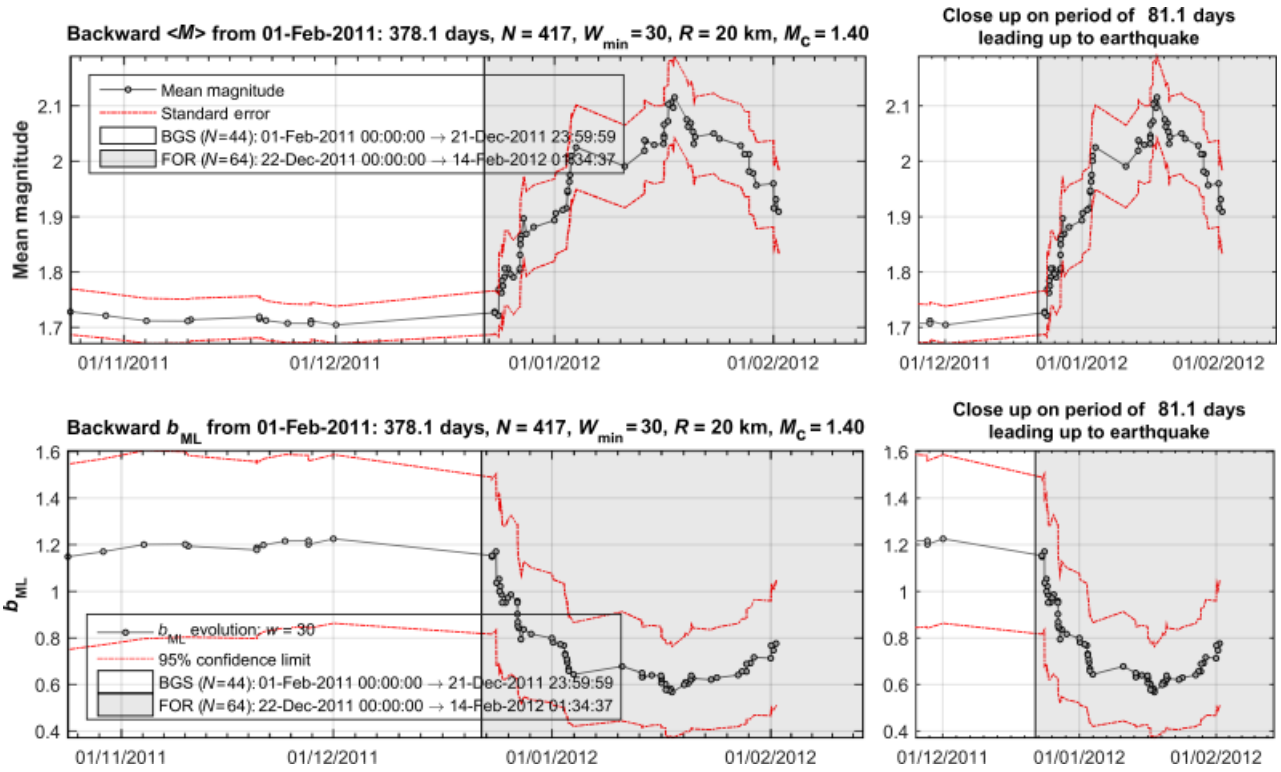

Figure 8.10 Time variation of (top) mean magnitude, <*M*>, and (bottom) b_{ML} of earthquake events of $M \geq M_c = 1.40$ occurring in the target area ($R = 20$ km) around the target point. Both parameters were calculated with the backward technique by considering $w = 30$ events starting from the origin time of the *Mw* 5.1 earthquake of 14 February 2012 and using a step of 1 event.

three-dimensional foreshock patterns. With this event the foreshock sequence entered in its strong stage culminating with the event of 4 March 2012, which was the strongest in the sequence. The entire foreshock sequence lasted for about 2.3 months, while the strong foreshock stage lasted for about 18 days. These time intervals are compatible with the duration of foreshock sequences preceding larger events (Table 8.1).

8.5.2. Polyphyto Area, North Greece, 3 July 2013, *Mw* 4.8

On 2 and 3 July 2013 two small-to-moderate earthquakes measuring magnitudes *Mw* 4.7/M_L 4.7 and *Mw* 4.8/M_L 4.7 occurred in the area of Polyphyto city, northern Greece (Table 8.1, Figure 8.11). This event is of particular interest because the area is considered to have a low level of seismic activity, but a very strong (*Mw* 6.6) earthquake struck on 13 May 1995. It is noteworthy that the area is characterized by the presence of the nearby Polyphyto artificial lake. In about the last 30 min before the 1995 main shock some foreshocks were recorded to the south of the source [*Drakatos et al.*, 1998] forcing residents to move outdoors, thus no one was killed [*Pavlides et al.*, 1995] in spite of the extensive building damage caused. The earthquakes of the 2 and 3 July 2013 took place at the southwestern tip of the artificial lake.

In our analysis we again considered an initial area of radius of 50 km around the epicenter of the main event of 3 July 2013. We found that from 8 November 2012 onwards the seismicity significantly clustered around the main event epicenter at a distance of < 25 km (Figure 8.12). This result is independent of the number of events used to calculate the mean distance, *D*, of earthquake epicenters from the main event epicenter (Figure 8.13).

During the last days before the main event a cluster developed very close to main event epicenter due to activity associated with the *Mw* 4.8 earthquake of 2 July. The analysis used here for the investigation of seismicity changes in the time and size domains is the same as that performed in the case of the Athos moderate earthquake event of 4 March 2012. The background and testing periods were considered as extending from 1 February 2011 up to 7 November 2012 and from 8 November 2012 up to the occurrence of the 3 July 2013 main event, which was the largest in the sequence. Seismicity analysis was performed

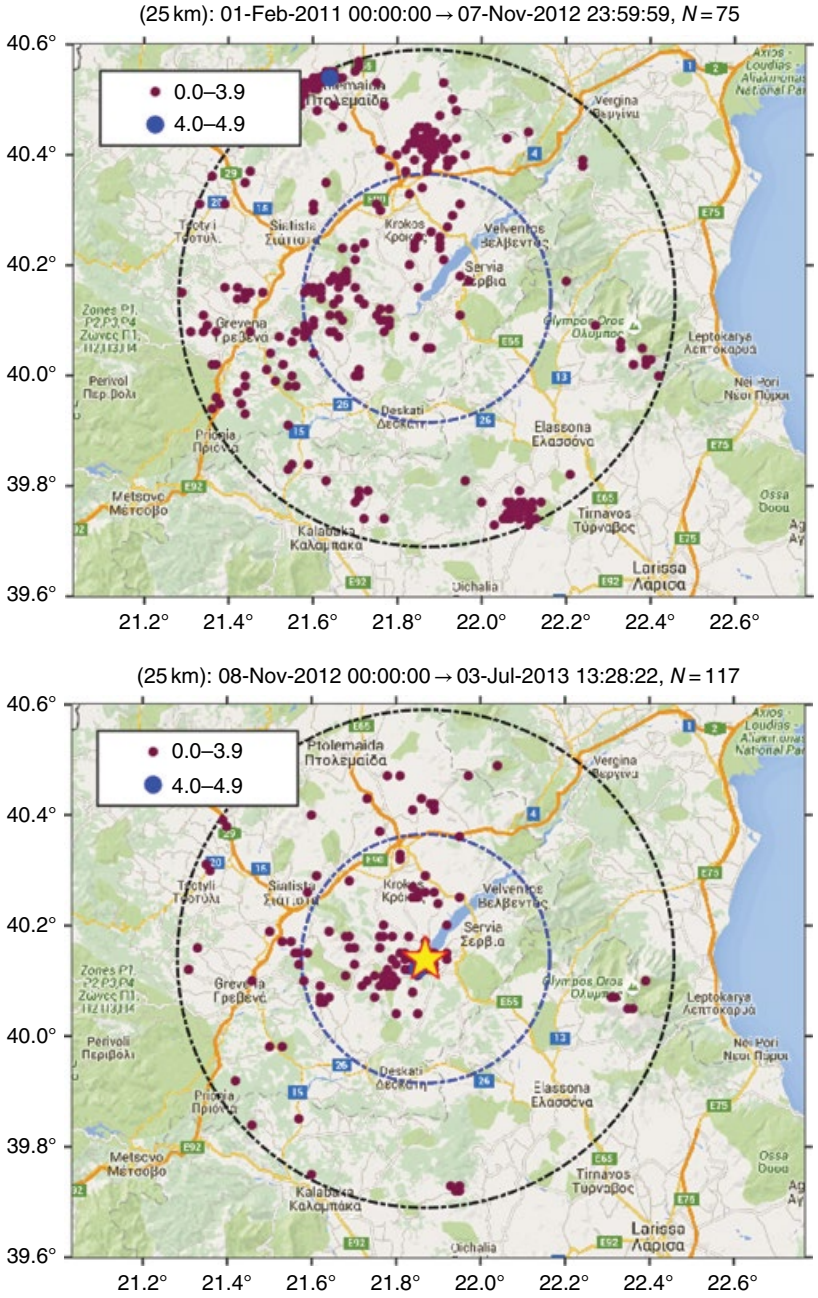

Figure 8.11 Earthquake epicenter plots in the Polyphyto area, northern Greece, for two time periods: (top) from 1 February 2011 to 7 November 2012 and (bottom) from 8 November 2012 to 3 July 2013. Circles are radii of 50 and 20 km from the epicenter of the 4 March 2013 main event (star). After 7 November 2012 the seismicity was clustered close to the main event epicenter at the southwestern tip of the Polyphyto artificial lake.

for magnitude cut-off $M_c = 1.10$ (Figure 8.14, top) in a target area of radius 25 km from the epicenter of the main event.

A significant (level of 98.54%) seismicity rate increase from $r_b = 0.12$ events day^{-1} to $r_f = 0.49$ events day^{-1} in the background and foreshock periods, respectively, was found (Figure 8.15). At the same time b_{ML} decreased from 0.77 to 0.59 (Figure 8.14, top) while the mean magnitude $< M >$ increased (Figure 8.16). The Utsu test showed $P = 0.09$. The b-value decrease is not highly significant due to the relatively small number of events, $N_b = 70$ and $N_f = 115$, contained in the two earthquake samples examined (Figure 8.14, top).

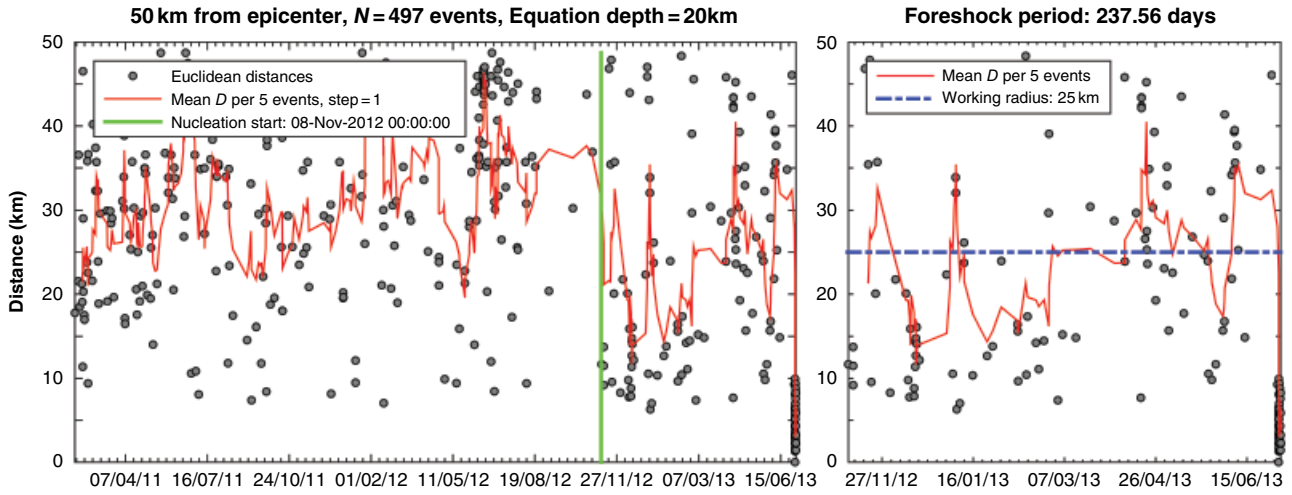

Figure 8.12 Time variation of the average Euclidean distance, *D*, of epicenters from that of the main event of 3 July 2013. At each point of time *D* was calculated as the average of five events.

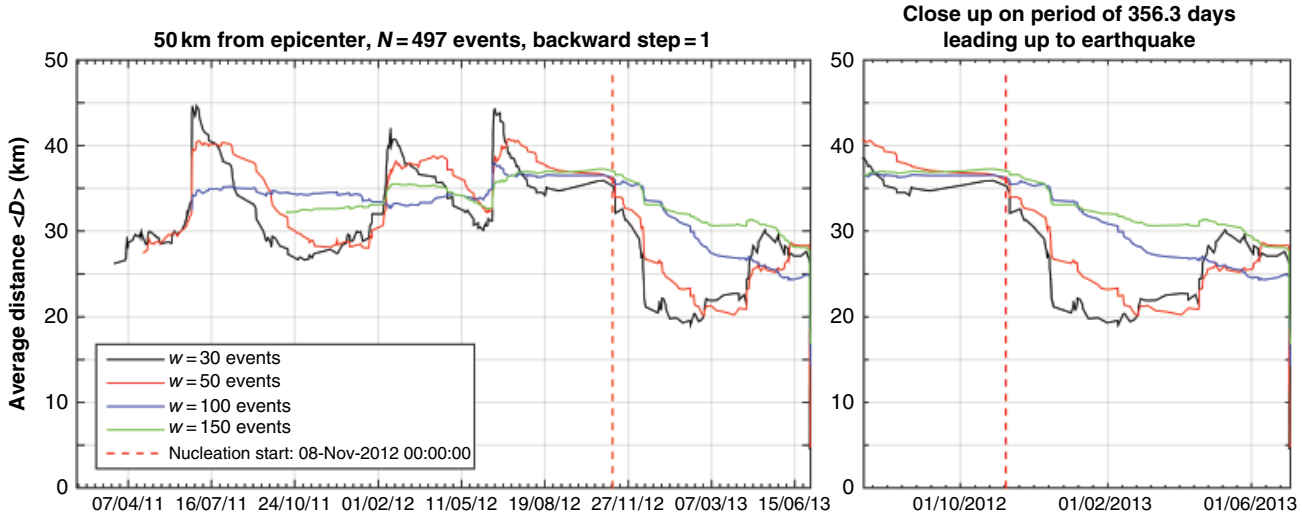

Figure 8.13 Time variation of the average Euclidean distance, *D*, of epicenters from that of the main event of 3 July 2013. At each point of time *D* was calculated with the backward technique as the average of *n* events (*n* was equal to 30, 50, 100, or 150) starting from the origin time of the 3 July 2013 main event and using a step of 1 event.

We note once more that a small-to-moderate event of *Mw* 4.8 was preceded by space, time and size patterns similar to the patterns found in foreshock sequences before larger main shocks. A characteristic feature of the Polyphyto case is the relatively long foreshock sequence, which lasted for nearly 8 months. Considering that the event ($Mw = 4.7$) of 2 July 2012 was the strongest foreshock, then the duration of the strong foreshock stage was of about only 27 h. Similarly to the Athos 2013 case, the two stronger events in the Polyphyto earthquake sequence have a very small difference in magnitude. Therefore, we again tested for the case that the first event (2 July 2012) was the main shock and that of 3 July 2012 was a strong aftershock. We found that the foreshock activity that preceded the event of 2 July 2012 was significant at the 91.47% level for the increase in activity rate from 0.13 to 0.25. However, the b_{ML} decrease from 0.77 to 0.63 was of low significance ($P = 0.195$). These features imply that the 8-month part of the activity represents the weak stage of the foreshock sequence.

8.6. DISCUSSION AND CONCLUSIONS

A series of critical issues regarding foreshocks and their value for earthquake prediction are still debatable. A review on the foreshock rate showed that contradictory results were obtained by different studies that examined different time periods of seismicity in various regions of

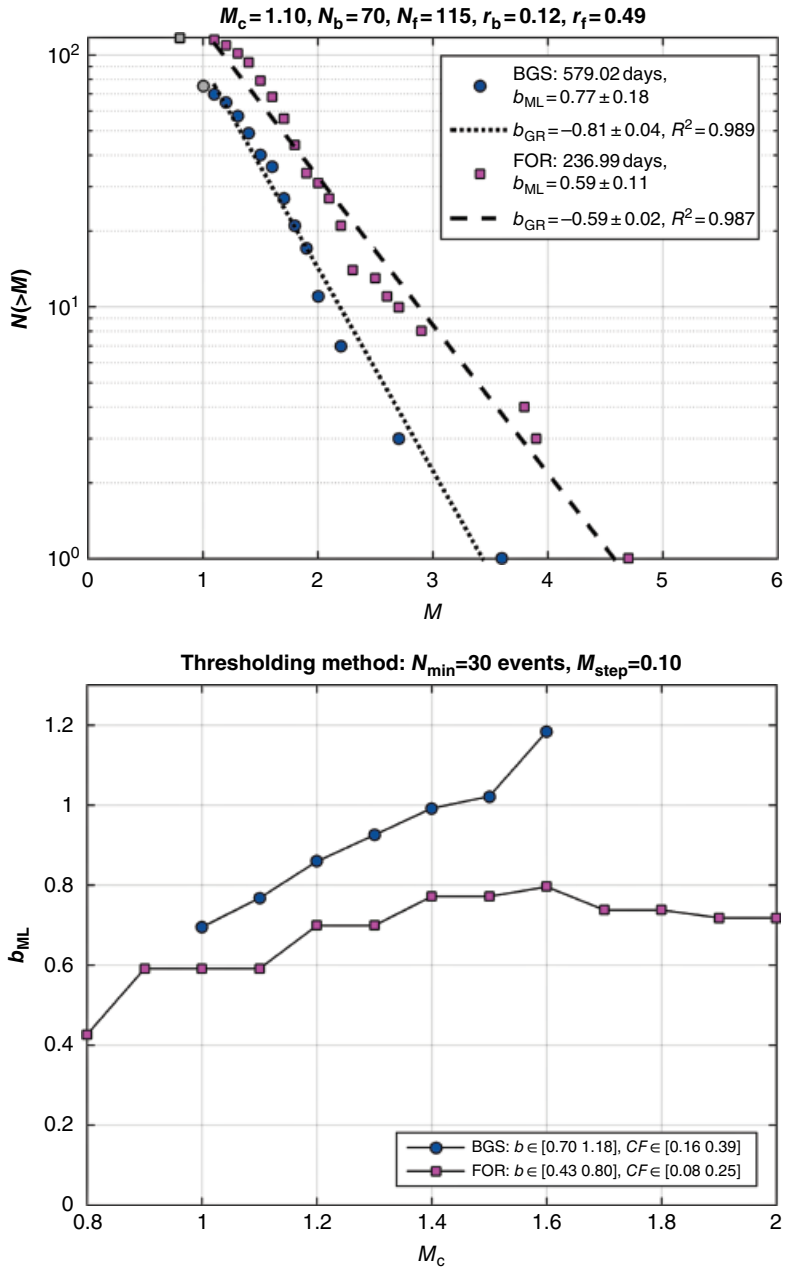

Figure 8.14 (Top) Magnitude–frequency (G–R) distribution of earthquakes occurring in the background seismicity period (BGS) and the foreshock period (FOR) before the main event of 3 July 2013. Notation as in Figure 8.6. In the foreshock period the b_{ML} remains lower than that in the background period for different M_c levels (bottom). Calculation performed for N_{min}=30 with a magnitude step of 0.10.

the Earth. It has been shown that the foreshock rate depends not only on crustal properties, such as material heterogeneity, focal depth and fault type, but also on the completeness of the earthquake catalog used and on the foreshock definition adopted. An important lesson learned is that foreshocks may escape recognition if the investigation focus is very narrow in space and time limits and/or the catalog magnitude cut-off is large. Also debatable is the issue of how foreshock incidence scales with the main shock size. So far it has generally been thought that foreshocks may precede only strong and large earthquakes, but very little knowledge is available on foreshock activity documented before moderate or small earthquakes [e.g. *Engdahl and Kisslinger*, 1978].

To our knowledge this is the first time that significant three-dimensional foreshock patterns have been investigated before small-to-moderate main shocks, such as the two Greek cases examined in this paper. This investigation

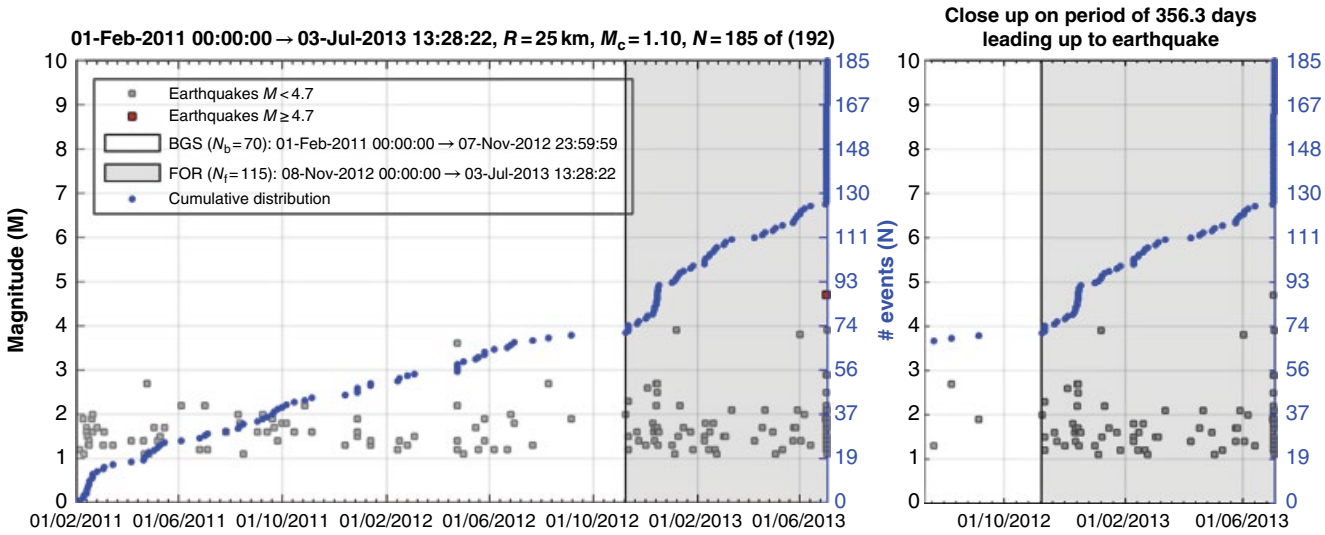

Figure 8.15 Cumulative number of earthquake events of magnitude $M \geq M_c = 1.10$ occurring in the target area ($R = 25$ km) around the epicenter of the main event of 4 March 2012. See Figure 8.4 for notation.

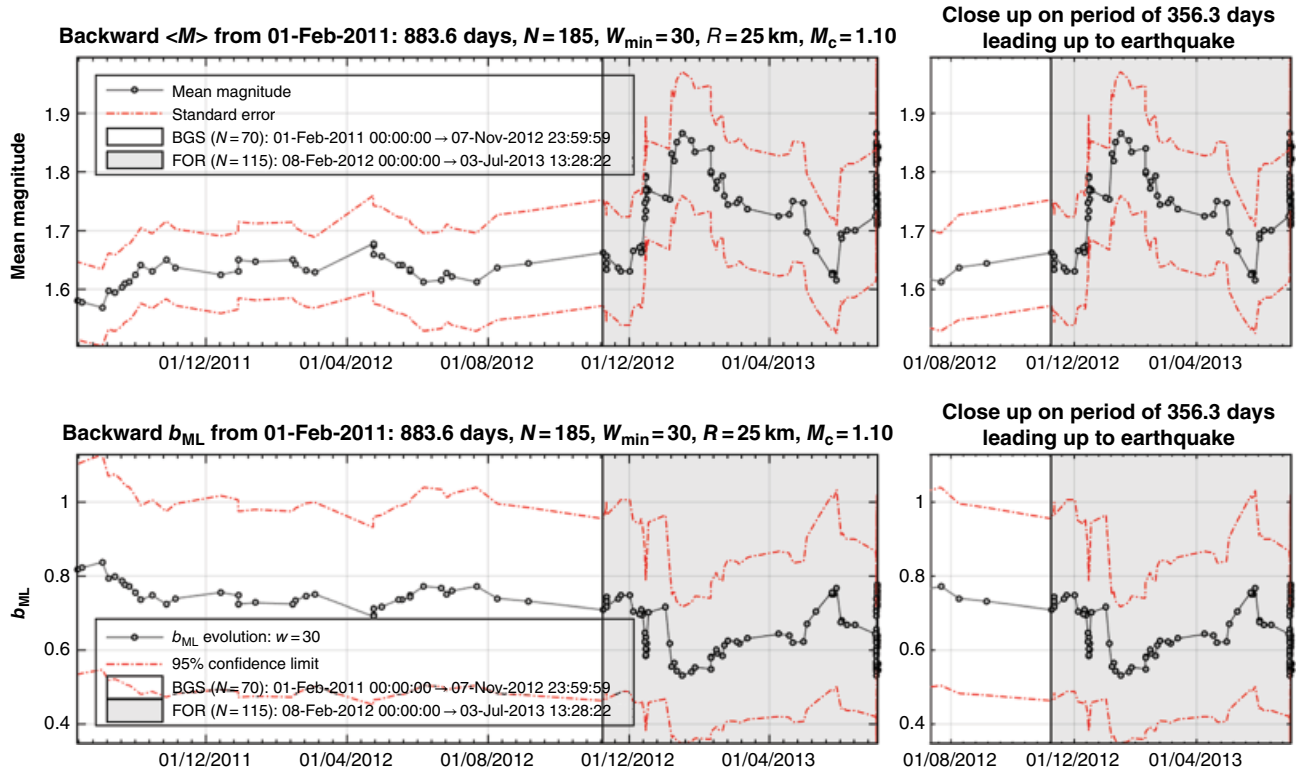

Figure 8.16 Time variation of (top) mean magnitude, <*M*>, and (bottom) b_{ML} of earthquake events with magnitude $M \geq M_c = 1.10$ occurring in the target area ($R = 25$ km) around the epicenter of the main event of 3 July 2013.

showed that in both cases, 4 March 2012 in Athos and 3 July 2013 in Polyphyto, the main events of *Mw* 5.2 and *Mw* 4.8, respectively, were preceded by foreshock sequences having three-dimensional patterns quite similar to the patterns that preceded strong and large main shocks. Investigation of foreshock activity occurring before earthquakes of moderate or even small magnitude may introduce new possibilities for better understanding the factors that likely control foreshock incidence and three-dimensional foreshock patterns. It is also of great

benefit for exploring universality in foreshock processes, i.e., whether patterns recognized before strong and large earthquakes can be also recognized in smaller magnitude main shocks.

Table 8.1 summarizes the main shock and foreshock parameters of the Athos and Polyphyto cases, of the L'Aquila (Italy) strong 2009 earthquake, and of three great earthquakes occurring in Chile in 2010, 2014 and 2015. This list contains only foreshock cases with three-dimensional patterns tested for statistical significance. Of particular importance is to consider the seismic fault types associated with the main shocks listed in Table 8.1. There is a general consensus that the L'Aquila 2009 main shock was associated with a normal fault striking NW–SE [e.g. *Chiarabba et al*., 2009; *Tinti et al*., 2014]. Moment tensor solutions produced by NOA (http://bbnet.gein.noa.gr/HL/database) indicated that both the Athos 2012 and Polyphyto 2013 small-to-moderate events in North Greece were also associated with normal faults striking NW–SE in Athos and NE–SW in Polyphyto. In contrast, thrust-type faulting has been recognized for the great Chilean subduction earthquakes of Maule 2010 [*Madariaga et al*., 2010], Iquique 2014 [*Schurr et al*., 2014] and Illapel 2015 [*Ye et al*., 2016].

In four out of six cases the foreshock sequence developed in two sequential stages: first a weak stage followed by a strong stage. In the Chilean cases of 2010 and 2015, however, the strong foreshock stage was lacking, only the weak foreshock stage was detected. This has been attributed to the large magnitude cut-off in the earthquake catalog [*Papadopoulos and Minadakis*, 2016]. A common feature in the four sequences is that the strong foreshock stage lasted < 3 weeks, ranging in duration from about 18 days in Athos (Greece) 2012 and in Iquique (Chile) 2014, to only 1.1 days in Polyphyto (Greece) 2013. The total duration of the six foreshock sequences ranges from nearly 8 months in Polyphyto to about 2.3 months in Athos and Iquique. The long duration of the weak foreshock stage in Polyphyto is likely due to the low rate of tectonic loading in the area, as evident from the low level of background seismicity. We do not rule out, however, that the generation of the Polyphyto sequence might be associated with water loading changes in the nearby dam, a topic that we intend to investigate.

It is quite obvious that the total duration of foreshock sequences, as well as the duration of the strong foreshock stage, do not correlate with the main shock magnitude, M_o, and the maximum foreshock magnitude, M_f. In addition, no correlation is evident between M_o and M_f, a result also found by other studies in the past.

Additionally, it is of interest to examine whether or not the main shock magnitude M_o scales with the surface of the foreshock area measured by radius R in Table 8.1. There is a tendency of M_o to scale with R but the Illapel (Chile, M_o 8.4) 2015 case is a possible deviation. In this case the foreshock area is smaller than that found for the Iquique (Chile, M_o 8.1) 2014 case. This again is possibly due to the higher magnitude cut-off in the Illapel case as compared to the Iquique case. Another problem is the accuracy of epicenter determination, particularly for lower magnitude events such those of Athos and Polyphyto in Greece. Relocation of foreshock sequences would help substantially to improve the estimation of the foreshock area.

Our conclusions are summarized as follows.

1. The estimation of the foreshock rate remains a debatable issue since it is not controlled only by geophysical factors, such as stress conditions, material heterogeneity, focal depth and fault type, but depends also on catalog completeness and the foreshock definition adopted.

2. When present, foreshock sequences likely follow certain three-dimensional patterns in the space, time and size domains: foreshock epicenters move towards the main shock epicenter, the event count increases as the inverse of time towards the main shock origin time, while the *b*-value decreases, and the mean magnitude $< M > (\sim 1/b)$ increases, with respect to that in background seismicity. However, only very few cases of single foreshock sequences were known so far to follow these three patterns at the same time: the L'Aquila 2009 (central Italy) case which concluded with a strong (*Mw* 6.3) main shock as well as the Chilean cases of Maule 2010, Iquique 2014, and Illapel 2015, which concluded with great earthquakes of Mw 8.8, 8.1, and 8.4, respectively. However, no foreshock sequence before small-to-moderate earthquakes was recognized previously.

3. For the first time in this paper we investigated foreshock sequences preceding small-to-moderate earthquakes. We examined the cases of Athos (*Mw* 5.2) and Polyphyto (*Mw* 4.8), both occurring in northern Greece on 4 March 2012 and 3 July 2013, respectively. It was found that both earthquakes were preceded by statistically significant three-dimensional foreshock patterns quite similar to those found before the L'Aquila strong main shock and the three Chilean great earthquakes.

4. The three-dimensional patterns appear independent of the seismic fault type, given that the Athos, Polyphyto, and L'Aquila main shocks were associated with crustal normal faulting while the three great Chilean earthquakes were typical subduction thrusts.

5. Usually the foreshock sequence developed as a weak stage followed by a strong stage. In the Chilean cases of 2010 and 2015, however, only the weak foreshock stage was detected. The lack of a strong foreshock stage is possibly explained by the large magnitude cut-off in the earthquake catalog. The four sequences comprising a strong foreshock stage lasted between 18 days in Athos (Greece) 2012 and in Iquique (Chile) 2014 and 1.1 days in

Polyphyto (Greece) 2013. The total duration of the six foreshock sequences varies from nearly 8 months in Polyphyto to nearly 2.3 months in Athos and Iquique. Further research is needed to explain the long duration of the weak foreshock stage in Polyphyto.

6. The total foreshock sequence duration and the duration of the strong foreshock stage do not correlate with the main shock magnitude, M_o, and the maximum foreshock magnitude, M_f. Also, the magnitudes M_o and M_f do not correlate.

7. There is a trend, however, for M_o to scale with the foreshock area, although the Illapel (Chile, M_o 8.4) 2015 case is a deviation, possibly due to the relatively high magnitude cut-off in the earthquake catalog of the Illapel area.

Our main finding is that the foreshock patterns in space, time and size domains are likely governed by scale-invariant universality holding in a very wide magnitude spectrum and for at least dip-slip fault types. Should this be a valid result it may indicate that the foreshock incidence is an inherent property of the deformation process leading to the main shock nucleation. Therefore, the results obtained above underline the need to further verify the hypothesis of scale-invariant universality of the foreshock three-dimensional patterns. Towards this aim the investigation of more good examples of statistically significant patterns occurring before earthquakes of various magnitudes and associated with various faulting types becomes a priority in foreshock research.

ACKNOWLEDGMENTS

This is a contribution to the Project "Pilot Study in the Area of Early Warning System for Natural Disasters: ARISTOTLE" funded by the EU DG-ECHO (contract n. ECHO/SER/2015/722144).

REFERENCES

Abercrombie, R. E. and Mori, J. (1996), Occurrence patterns of foreshocks to large earthquakes in the western United States, *Nature*, *381*, 303–307.

Agnew, D. C. and Jones, L. (1991), Prediction probabilities from foreshocks. *J. Geophys. Res.*, *96*(B7), 11959–11971.

Aki, K. (1965), Maximum likelihood estimates of *b* in the formula $\log N = a - bM$ and its confidence limits, *Bull. Earth. Res. Inst. Univ. Tokyo*, *43*, 237–239.

Avlonitis, M. and Papadopoulos, G. A. (2014), Foreshocks and *b* value: bridging macroscopic observations to source mechanical considerations, *Pure Appl. Geophys.*, *17S1*(10), 2569–2580, doi: 10.1007/s00024-014-0799-6

Bedford, J., Moreno, M., Schurr, B., Bartsch, M., and Oncken, O. (2015), Investigating the final seismic swarm before the Iquique-Pisagua 2014 *Mw* 8.1 by comparison of continuous GPS and seismic foreshock data. *Geophys. Res. Lett.*, *42*, doi:10.1002/2015GL063953.

Bouchon, M., Durand, V., Marsan, D., Karabulut, H., and Schmittbuhl, J., 2013, The long precursory phase of most large interplate earthquakes, *Nature Geosci.*, *6*(4), 299–302, doi 10.1038/ngeo1770.

Brodsky, E. and Lay, Th. (2014), Recognizing foreshocks from the 1 April 2014 Chile earthquake, *Science*, *344*, 700–702.

Chan, C-H, Wu, Y-M., Tseng, T-L., Lin, T-L., and Chen, C.-C. (2012), Spatial and temporal evolution of b-values before large earthquakes in Taiwan, *Tectonophysics*, *532–535*, 215–222, doi:10.1016/j.tecto.2012.02.004

Chen, Y., Liu, J., and Ge, H., (1999), Pattern characteristics of foreshock sequences, *Pure Appl. Geophys.*, *155*, 2–4, 395–408.

Cheng, Y. and Wong, L. N. Y. (2016), Occurrence of foreshocks in large earthquakes with strike-slip rupturing, *Bull. Seism. Soc. Am.*, *106*, 213–224, doi:10.1785/0120140338.

Chiarabba, C., Amato, A., Anselmi, M., et al., (2009), The 2009 L' Aquila (central Italy) Mw6.3 earthquake: Main shock and aftershocks, *Geophys. Res. Lett.*, *36*, L18308, doi: 10.1029/2009GL039627

Console, R., Murru, M., and Alessandrini, B. (1993), Foreshock statistics and their possible relationship to earthquake prediction in the Italian region. *Bull. Seismol. Soc. Am.*, *83*, 1248–1263.

Daskalaki, E., Spiliotis, K., Siettos, C., Minadakis, G., and Papadopoulos, G. A. (2016), Foreshocks and short-term hazard assessment to large earthquakes using complex networks: the case of the 2009 L'Aquila earthquake, *Nonlin. Processes Geophys.*, *23*, 241–256, https://doi.org/10.5194/npg-23-241-2016

Di Luccio, F., Console, R., Imoto, M., and Murru, M. (1997), Analysis of short time-space range seismicity patterns in Italy, *Ann. di Geofis.*, *XL*, 783–798.

Dodge, D. A., Beroza, G. C., and Ellsworth, W. L. (1995), Foreshock sequence of the 1992 Landers, California, earthquake and its implications for earthquake nucleation. *J. Geophys. Res.*, *100*(B6), 9865–9880.

Doser, D. (1989), Foreshocks and aftershocks of large ($M \geq 5.5$) earthquakes within the western Cordillera of the United States, *Bull. Seismol. Soc. Am.*, *80*, 110–128.

Drakatos, G., Papanastassiou, D., Papadopoulos, G., Skafida, H., and Stavrakakis, G., (1998), Relationship between the 13 May 1995 Kozani-Grevena (NW Greece) earthquake and the Polyphyto artificial lake. *Eng. Geol.*, *51*, 65–74.

Duputel, Z., Jiang, J., Jolivet, R. et al. (2015), The Iquique earthquake sequence of April 2014: Bayesian modeling accounting for prediction uncertainty, *Geophys. Res. Lett.*, *42*, 7949–7957, doi:10.1002/2015GL065402

Engdahl, E. R. and Kisslinger, C. (1978), Seismological precursors to a magnitude 5 earthquake in the Central Aleutian Islands, in C. Kisslinger and Z. Suzuki (eds), *Earthquake Precursors*, pp. 243–250, Center for Academic Publications, Tokyo.

Frohlich, C. and Davis, S. D. (1993), Teleseismic *b* values; or, much ado about 1.0. *J. Geophys. Res.*, *98*(B1), 631–644.

Gutenberg, B. and Richter, C. (1944), Frequency of earthquakes in California, *Bull. Seismol. Soc. Am.*, *34*, 185–188.

Hainzl, S., Zoller, G., and Kurths, J. (1999), Similar power laws for foreshock and aftershock sequences in a spring-block model for earthquakes, *J. Geophys. Res.*, *104*, 7243–7253.

Hamilton, R. M. (1967), Mean magnitude of an earthquake sequence. *Bull. Seismol. Soc. Am.*, *57*, 1115–1116.

Imamura, A., (1937), *Theoretical and Applied Seismology*, Maruzen, Tokyo, 358 pp.

Imoto, M. (2005), *Use of Potential Foreshocks to Estimate the Short-Term Probability of Large Earthquakes*, Tohoku, Japan.

Ishida, M. and Kanamori, H. (1978), The foreshock activity of the 1971 San Fernando earthquake, California. *Bull. Seismol. Soc. Am.*, *68*, 1265–1279.

Ishimoto, M. and Iida, K. (1939), Observations of earthquakes registered with the microseismograph constructed recently, *Bull. Earthquake Res. Inst. Tokyo Univ.*, *17*, 443–478.

Jones, L. M. (1985a), Foreshocks and time-dependent earthquake hazard assessment in southern California, *Bull. Seismol. Soc. Am.*, *75*(6), 1669–1679.

Jones, L. M. (1985b), Foreshocks (1966–1980) in the San Andreas system California. *Bull. Seismol. Soc. Am.*, *74*, 1361–1380.

Jones, L. M. and Molnar, P. (1976), Frequency of foreshocks, *Nature*, *262*(5570), 677–679.

Jones, L. M. and Molnar, P. (1979), Some characteristics of foreshocks and their possible relationship to earthquake prediction and premonitory slip on faults, *J. Geophys. Res.*, *84*, 3596–3608.

Jones, L. M., Wang, B., Xu, S., and Fitch, Th.-J., (1982), The foreshock sequence of the February 4, 1975, Haicheng earthquake ($M = 7.3$). *J. Geophys. Res.*, *87*(B6), 4575–4584.

Kagan, Y. and Knopoff, L. (1978), Statistical study of the occurrence of shallow earthquakes, *Geophys. J. Roy. Astr. Soc.*, *55*, 67–86.

Kato, A. and Nakagawa, S. (2014), Multiple slow-slip events during a foreshock sequence of the 2014 Iquique, Chile *Mw* 8.1 earthquake, *Geophys. Res. Lett.*, *41*, 5420–5427, doi: 10.1002/2014GL061138

Kato, A., Obara, K., Igarashi, T., Tsuruoka, H., Nakagawa, S., and Hirata N. (2012), Propagation of slow slip leading up to the 2011 *Mw* 9.0 Tohoku-Oki earthquake, *Science*, *335*(6069), 705–708.

Lay, Th., Yue, H., Brodsky, E. E., and An, C., (2014), The 1 April 2014 Iquique, Chile, *Mw* 8.1 earthquake rupture sequence, *Geophys. Res. Lett.*, *41*, doi:10.1002/2014GL060238.

Lin, C.-H., (2004), Repeated foreshock sequences in the thrust faulting environment of eastern Taiwan. *Geophys. Res. Lett.*, *31*, L13601, doi:10.1029/2004GL019883

Lippiello, E., Marzocchi, W., De Arcangelis, L., and Godano, C. (2012), Spatial organization of foreshocks as a tool to forecast large earthquakes, *Sci. Rep.*, *2*, DOI:10.1038/srep00846.

Lomnitz, C. (1966), Magnitude stability in earthquake sequences. *Bull. Seismol. Soc. Am.*, *56*, 247–249.

Madariaga, R., Métois, M., Vigny, Ch., and Campos, J. (2010), Central Chile finally breaks, *Science*, *328*, 181–182, doi: 10.1126/science.1189197

Maeda, K. (1999), Time distribution of immediate foreshocks obtained by a stacking method, *Pure Appl. Geophys.*, *155*(2–4), 381–394.

Main, I. (2000), Apparent breaks in scaling in the earthquake cumulative frequency-magnitude distribution: fact or artifact? *Bull. Seismol. Soc. Am.*, *90*(1), 86–97.

Main, I., Meredith, Ph. G., and Jones, C. (1989), A reinterpretation of the precursory seismic b-value anomaly from fracture mechanics, *Geophys. J. Int.*, *96*, 131–138.

Meng, L., Huang, H., Bürgmann, R., Ampuero, J.-P., and Strader, A. (2015), Dual megathrust slip behaviors of the 2014 Iquique earthquake sequence, *Earth Planet. Sci. Lett.*, *411*, 177–187.

Merrifield, A., Savage, M. K., and Vere-Jones, D., (2004), Geographical distributions of prospective foreshock probabilities in New Zealand, *N. Z. J. Geol. Geophys.*, *47*, 327–339.

MichaeL, A. (2012), Fundamental questions of earthquake statistics, source behavior, and the estimation of earthquake probabilities, *Bull. Seismol. Soc. Am.*, *102*, 2547–2562, doi: 10.1785/0120090184.

Mogi, K. (1963a), The fracture of a semi-infinite body caused by an inner stress origin and its relation to the earthquake phenomena (second paper), *Bull. Earthquake Res. Inst. Univ. Tokyo*, *41*, 595–614.

Mogi, K. (1963b), Some discussion on aftershocks, foreshocks and earthquake swarms – the fracture of a semi-infinite body caused by an inner stress origin and its relation to the earthquake phenomena (third paper), *Bull. Earthquake Res. Inst. Univ. Tokyo*, *41*, 615–658.

Mogi, K. (1985), *Earthquake Prediction*, Academic Press, Tokyo, 355 pp.

Molchan, G. M., Kronrod, T. L., and Nekrasona, A. K. (1999), Immediate foreshocks: time variation of the *b*-value, *Phys. Earth Planet. Int.*, *111*, 229–240.

Nanjo, K. Z., Hirata, N., Obara, K., and Kasahara, K. (2012), Decade-scale decrease in *b* value prior to the *M*9-class 2011 Tohoku and 2004 Sumatra quakes, *Geophys. Res. Lett.*, *39*, L20304, doi:10.1029/2012GL052997

Ogata, Y., Utsu, T., and Katsura, K. (1996), Statistical discrimination of foreshocks from other earthquake clusters, *Geophys. J. Int.*, *127*, 17–30.

Papadopoulos, G. A., Drakatos, G., and Plessa, A. (2000), Foreshock activity as a precursor of strong earthquakes in Corinthos Gulf, Central Greece, *Phys. Chem. Earth*, *25*, 239–245.

Papadopoulos, G. A., Charalampakis, M., Fokaefs, A., and Minadakis, G. (2010), Strong foreshock signal preceding the L'Aquila (Italy) earthquake (*Mw* 6.3) of 6 April 2009. *Nat. Hazards Earth Syst. Sci.*, *10*, 19–24.

Papadopoulos, G. A., Latoussakis, I., Daskalaki, E., Diakogianni, G., Fokaefs, A., Kolligri, M., Liadopoulou, K., Orfanogiannaki, K., and Pirentis, A. (2006), The East Aegean Sea strong earthquake sequence of October–November 2005: lessons learned for earthquake prediction from foreshocks, *Nat. Hazards Earth Syst. Sci.*, *6*, 895–901.

Papadopoulos, G. A. and Minadakis, G. (2016), Foreshock patterns preceding great earthquakes in the subduction zone of Chile, *Pure Appl. Geophys.*, *173*(10–11), 3247–3271.

Papazachos, B. C. (1974), Dependence of the seismic parameter *b* on the magnitude range, *Pure Appl. Geophys.*, *112*, 1059–1065.

Papazachos, B. C. (1975), Foreshocks and earthquake prediction, *Tectonophysics*, *28*, 213–226.

Pavlides, S. B., Zouros, N. C., Chatzipetros, A. A., Kostopoulos, D. S., and Mountrakis, D. M., (1995), The 13 May 1995 western Macedonia, Greece (Kozani-Grevena) earthquake: preliminary results, *Terra Nova*, *7*, 544–549.

Peçi, V., Maeda, K., Matsumura, K., and Irikura, K. (1999). Foreshock activity and its probabilistic relation to earthquake occurrence in Albania and the surrounding area, *Ann. di Geofis.*, *42*, 809–819.

Raleigh, B., Benett, G., Craig, H. et al. (1977), Prediction of the Haicheng earthquake, *EOS (Trans. Am. Geophys. Union)*, *58*, 236–272.

Ruiz, S., Metois, M., Fuenzalida, A. et al. (2014), Intense foreshocks and a slow slip event preceded the 2014 Iquique *Mw* 8.1 earthquake, *Science*, doi:10.1126/science.1256074

Savage, M. K. and DePolo, D. M., (1993), Foreshock probabilities in the western great-basin eastern Sierra Nevada, *Bull. Seismol. Soc. Am.*, *83* (6), 1910–1938.

Scholz, C. H. (1968), Microfractures, aftershocks, and seismicity, *Bull. Seismol. Soc. Am.*, *58*, 1117–1130.

Scholz, C. H. (1977), A physical interpretation of the Haicheng earthquake prediction, *Nature*, *267*, 121–124.

Schorlemmer, D., Wiemer, S., and Wyss, M. (2005), Variations in earthquake-size distribution across different stress regimes, *Nature*, *437*, 539–542.

Schurr, B., Asch, G., Hainzl, S. et al. (2014), Gradual unlocking of plate boundary controlled initiation of the 2014 Iquique earthquake, *Nature*, *512*, 299–302, doi: 10.1038/nature13681

Seggern, D. (1981), Seismicity pattern preceding moderate to major earthquakes, *J. Geophys. Res.*, *86* (B10), 9325–9351.

Sobolev, G. A. (2000), Precursory phases of large Kamchatkan earthquakes, *Volcanol. Seismol.*, *21*, 497–509.

Suyehiro, S. (1966), Difference between aftershocks and foreshocks in the relationship of magnitude to frequency of occurrence for the great Chilean earthquake of 1960, *Bull. Seismol. Soc. Am.*, *56*, 185–200.

Suyehiro, S. and Sekiya, H. (1972), Foreshocks and earthquake prediction, *Tectonophysics*, *14*, 219–225.

Suyehiro, S., Asada, T., and Ohtake, M. (1964), Foreshocks and aftershocks accompanying a perceptible earthquake in central Japan, *Meteorol. Geophys.*, *15*, 71–88.

Tinti, E., Scognamiglio, L., Cirella, A., and Cocco, M. (2014), Up-dip directivity in near-source during the 2009 L' Aquila main shock, *Geophys. J. Int.*, *198*, 1618–163, doi: 10.1093/gji/ggu227

Utsu, T. (1965), A method for determining the value of *b* in a formula $\log N = a - bM$ showing the magnitude–frequency relation for earthquakes, *Geophys. Bull. Hokkaido Univ.*, *13*, 99–103. (In Japanese.)

Utsu, T. (1966), A statistical test of the difference in *b*-value between two earthquake groups, *J. Phys. Earth*, *14*, 37–40.

Utsu, T. (1992), Representation and analysis of the earthquake size distribution: A historical review and some new approaches, *Pure Appl. Geophys.*, *155*, 509–535, 1992.

Vidale, J., Mori, J., and Houston, H., (2001), Something wicked this way comes: clues from foreshocks and earthquake nucleation, *EOS (Trans. Am. Geophys. Union)*, *82*, 68.

Wu, C., Meng, X., Peng, Z., and Ben-Zion, Y. (2014), Lack of spatiotemporal localization of foreshocks before the 1999 *Mw* 7.1 Düzce, Turkey, earthquake. *Bull. Seismol. Soc. Am.*, *104*, 560–566.

Wyss, M. (1997), Second round of evaluations of proposed earthquake precursors, *Pure Appl. Geophys.*, *149*, 3–16.

Yagi, Y., Okuwaki, R., Enescu, B. et al., (2014), Rupture process of the 2014 Iquique Chile earthquake in relation with the foreshock activity, *Geophys. Res. Lett.*, *41*, doi: 10.1002/2014GL060274

Yamaoka, K., Ooida T., and Ueda Y. (1999), Detailed distribution of accelerating foreshocks before a M 5.1 earthquake in Japan, *Pure Appl. Geophys.*, *155*(2–4), 335–353.

Yamashina, K. (1981), A method of probability prediction for earthquakes in Japan, *J. Phys. Earth*, *29*, 9–22.

Yamashita, T. and Knopoff, L., (2007), A model of foreshock occurrence, *Geophys. J. Int.*, *96*(3), 389–399.

Ye, L., Lay, Th., Kanamori, H., and Koper, K. D., (2016), Rapidly estimated seismic source parameters for the 16 September 2015 Illapel, Chile *Mw* 8.3 Earthquake. *Pure Appl. Geophys.*, *173*, 321–332, doi: 10.1007/s00024-015-1202-y